iScience

CellPress
OPEN ACCESS

Article

Interplay between FLI-1 and the LDB1 complex in murine erythroleukemia cells and during megakaryopoiesis

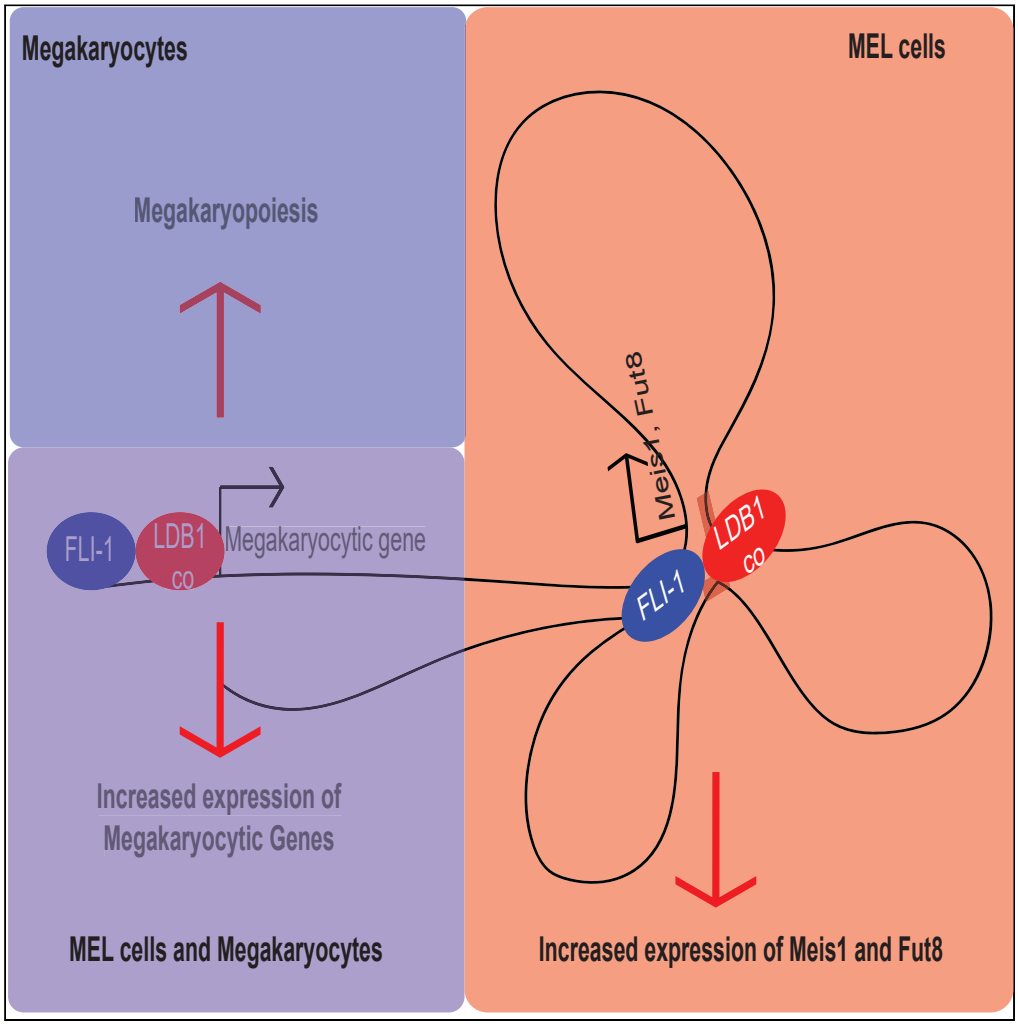

Guillaume Giraud, Petros Kolovos, Ilias Boltsis, ..., Wilfred van IJcken, François Morlé, Frank Grosveld

guillaume.giraud@inserm.fr (G.G.)
f.grosveld@erasmusmc.nl (F.G.)

HIGHLIGHTS

FLI-1 is important for the recruitment of the LDB1 complex

FLI-1 is important for chromatin looping

FLI-1 and the LDB1 complex co-regulate megakaryopoiesis

Giraud et al., iScience *24*, 102210
March 19, 2021
https://doi.org/10.1016/j.isci.2021.102210

iScience

CellPress
OPEN ACCESS

Article

Interplay between FLI-1 and the LDB1 complex in murine erythroleukemia cells and during megakaryopoiesis

Guillaume Giraud,[1,9,10,12,*] Petros Kolovos,[2,10] Ilias Boltsis,[1,10] Jente van Staalduinen,[1] Boris Guyot,[3,6,7,8,11] Michele Weiss-Gayet,[4,11] Wilfred van IJcken,[5] François Morlé,[4] and Frank Grosveld[1,*]

SUMMARY

Transcription factors are key players in a broad range of cellular processes such as cell-fate decision. Understanding how they act to control these processes is of critical importance for therapy purposes. FLI-1 controls several hematopoietic lineage differentiation including megakaryopoiesis and erythropoiesis. Its aberrant expression is often observed in cancer and is associated with poor prognosis. We showed that FLI-1 interacts with the LDB1 complex, which also plays critical roles in erythropoiesis and megakaryopoiesis. In this study, we aimed to unravel how FLI-1 and the LDB1 complex act together in murine erythroleukemia cells and in megakaryocyte. Combining omics techniques, we show that FLI-1 enables the recruitment of the LDB1 complex to regulatory sequences of megakaryocytic genes and to enhancers. We show as well for the first time that FLI-1 is able to modulate the 3D chromatin organization by promoting chromatin looping between enhancers and promoters most likely through the LDB1 complex.

INTRODUCTION

Transcription factors (TF) play critical roles in a broad range of cellular processes such as cell-fate decision and proliferation. They act as protein complexes to directly regulate gene expression through their recruitment to regulatory sequences. Their aberrant expression, which triggers perturbation in their molecular networks, is often the primary cause of cancer (Bhagwat and Vakoc, 2015; Nebert, 2002). Moreover, this class of proteins is also used as a cocktail of TF to reprogram differentiated cells into pluripotent stem cells (Rapino et al., 2013; Takahashi and Yamanaka, 2006). Therefore, understanding how TFs act to control these different processes remains critical to improve therapeutic strategies for cancer or for regenerative medicine.

Fli-1 TF belongs to the ETS family, whose members are characterized by a conserved ETS DNA-binding domain recognizing a purine-rich motif, GGAA (Wei et al., 2010). *Fli-1* was first identified as the main integration site of the Friend helper virus (F-MuLV), which triggers erythroleukemia in mice (Ben-David et al, 1990, 1991). In murine erythroleukemia (MEL) cells, Fli-1, together with another ETS TF, Pu.1, contributes to the proliferation, the survival, and the block of differentiation of erythroid progenitors (Juban et al., 2009). In humans, *Fli-1* aberrant expression is observed in autoimmune diseases as well as in hematopoietic and non-hematopoietic cancer and is often associated with poor prognosis (Kornblau et al., 2011; Suzuki et al., 2012; Yan et al., 2018). Next to this role in pathology, Fli-1 targeted mice display defects in several hematopoietic lineages such as granulocytes, erythrocytes, and megakaryocytes (Kawada et al., 2001; Masuya et al., 2005; Moussa et al., 2010; Spyropoulos et al., 2000). In particular, Fli-1 promotes megakaryopoiesis at the expense of erythropoiesis (Starck et al., 2010). Interestingly, Fli-1 has been used in combination with GATA1 and TAL1 TF to enhance megakaryocyte production from pluripotent stem cells, which has its importance in transfusion-based therapies (Moreau et al., 2016). Despite these well-established contributions of Fli-1 during physiological and pathological development, the molecular mechanisms by which this important TF acts still remain elusive.

GATA1 and TAL1 are part of a same protein complex, namely the LDB1 complex. This complex, which also contains the E2A TF and two bridge proteins, LDB1 and LMO2, act as a platform to recruit either co-activators or co-repressors to regulate gene expression (Love et al., 2014). The LDB1 complex is important at all

[1]Department of Cell Biology, Erasmus Medical Centre, 3015CN Rotterdam, the Netherlands

[2]Department of Molecular Biology and Genetics, Democritus University of Thrace, Alexandroupolis 68100, Greece

[3]CNRS UMR5286, Centre de Recherche en Cancérologie de Lyon, Lyon, France

[4]Institut NeuroMyoGène, CNRS UMR 5310 - INSERM U1217 - Université de Lyon - Université Claude Bernard Lyon 1, Lyon, France

[5]Biomics Center, Erasmus University Medical Center, 3015CN Rotterdam, the Netherlands

[6]Inserm U1052, Centre de Recherche en Cancérologie de Lyon, Lyon, France

[7]Université de Lyon, Lyon, France

[8]Department of Immunity, Virus and Microenvironment, Lyon, France

[9]Present address: INSERM U1052 – Cancer Research Center of Lyon, Lyon, France

[10]These authors contributed equally

[11]These authors contributed equally

[12]Lead contact

*Correspondence: guillaume.giraud@inserm.fr (G.G.), f.grosveld@erasmusmc.nl (F.G.)

https://doi.org/10.1016/j.isci.2021.102210

the steps of erythropoiesis including the expansion of erythroid progenitors and the terminal differentiation. To do so, the LDB1 complex is mainly recruited to enhancers of critical genes involved in these processes such as *c-Myb* or *ß-globin* and promotes chromatin looping to place these enhancers in close proximity to the targeted promoter to activate their expression (Krivega et al., 2014; Krivega and Dean, 2017; Lee et al., 2017; Li et al., 2013; Stadhouders et al, 2012, 2014; Soler et al., 2010). Next to this critical role during erythropoiesis, the LDB1 complex is also important for megakaryopoiesis (Hamlett et al., 2008). However, how it works in this context is not fully described yet.

We have previously shown that Fli-1 and the LDB1 complex interact in MEL cells (Giraud et al., 2014). We hypothesized that Fli-1 and the LDB1 complex control the expression of common target genes. We used MEL cells as a cellular model to decipher how Fli-1 works in combination with the LDB1 complex. By using omics techniques, we show that Fli-1 and the LDB1 complex are mainly recruited to active enhancers where Fli-1 enables the recruitment of the LDB1 complex and their chromatin looping to the corresponding promoter, which demonstrates for the first time a role of FLI-1 in the 3D structure of the genome. We also show that in MEL cells as in megakaryocytes, Fli-1 and the LDB1 complex directly activates the expression of megakaryocytic genes and that they cooperatively regulate megakaryopoiesis.

RESULTS

Fli-1 binds active regions containing the ETS and the TAL1:GATA1 motifs

To unravel the mode of action of FLI-1, we first performed Fli-1 ChIP-Seq in MEL cells. With a comprehensive bioinformatical analysis, we identified 1,116 Fli-1 genome-wide bound regions and verified them by ChIP-qPCR assays in non-induced and DMSO-induced MEL cells (Figures 1A and S1A). As expected, the depletion of Fli-1 by shRNA in both states decreases the signal observed in these regions highlighting its specificity (Figures S1A–S1C). Fli-1 binding regions are preferentially located at gene bodies (Figure 1B) and the majority is in regions marked by the H3K9Ac and H3K27Ac histone modifications, corresponding to active chromatin regions (Figure 1C). We identified the DNA-binding motifs in the vicinity of the Fli-1 bound regions and as expected based on previous studies, more than 95% of the Fli-1 binding regions are enriched for the ETS motif (Figures 1D and 1E) (Wei et al., 2010; Wilson et al., 2010). Strikingly, almost 60% of these Fli-1 binding regions have the TAL1:GATA1 motif (Love et al., 2014; Soler et al., 2010), which recruits the LDB1 complex suggesting that FLI-1 is recruited together with the LDB1 complex in its target regions (Figures 1D and 1E).

Taken together, these analyses show that Fli-1 binds active regions containing the ETS motif and the TAL1:-GATA1 motif.

Fli-1 and the LDB1 complex are mainly bound to active enhancers in MEL cells

Based on the abovementioned observations, we investigated whether Fli-1 and the LDB1 complex are recruited to common regions. We compared the Fli-1 genome-wide bound regions in MEL cells with those available for the LDB1 complex in the same cells (Soler et al., 2010). This analysis revealed that 449 regions recruit both Fli-1 and the LDB1 complex in MEL cells (Figures 2A and 2B). We confirmed by ChIP-qPCR the recruitment of the LDB1 complex on some FLI-1 binding regions (Figure S1D). Interestingly, although the Fli-1-bound regions without the LDB1 complex are mostly present at promoter regions, the 449 common binding regions are mostly present in intragenic and intergenic regions (Figure 2C). In agreement with this observation, the majority of the Fli-1-bound regions without the LDB1 complex are located at regions containing the H3K4me3, H3K9Ac, and H3K27Ac histone modifications corresponding to active promoters (Figure 2D). Although the majority of the commonly bound regions for Fli-1 and the LDB1 are marked by H3K9Ac and H3K27Ac histone signatures, they are almost always bound by the p300 acetyltransferase and are more often marked by H3K4me1 compared with the Fli-1 binding regions without the LDB1 complex (Figure 2D). These observations show that Fli-1 and the LDB1 complex mainly bind active enhancers.

Using comprehensive motif enrichment analyses, we identified that both Fli-1 only and common binding regions contain the ETS motif, as also identified above (Figures 2E and 2F). As expected, the common binding regions contain the TAL1:GATA1 motif when compared with the Fli-1-only binding regions (Figures 2E and 2F). This analysis also highlights the enrichment for other motifs such as RUNX1 or STAT3 motifs specifically found in the common binding regions, which suggests that these two TFs also contribute to the function of Fli-1 and the LDB1 complex.

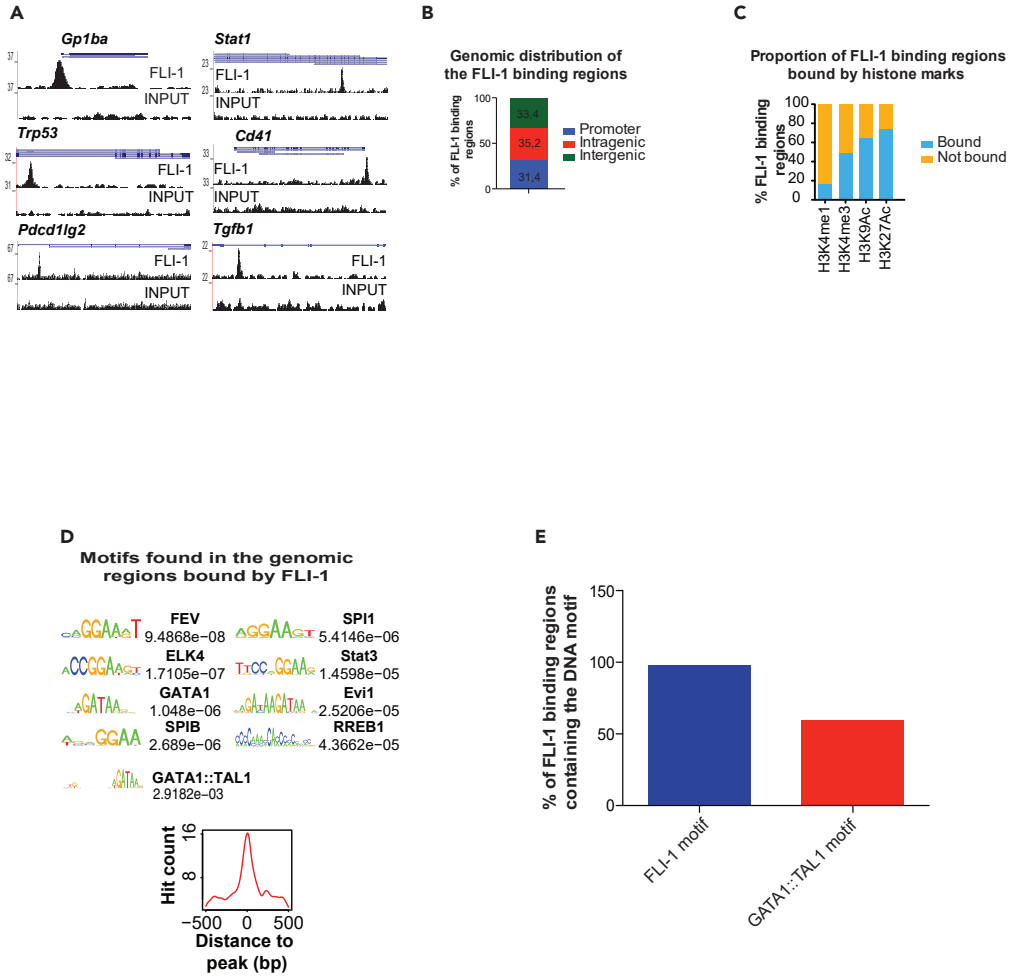

Figure 1. Fli-1 binds active regions containing the ETS and the TAL1:GATA1 motif in MEL cells

(A) Binding sites of Fli-1 observed in the Gp1ba, Stat1, Trp53, Cd41, Pdcd1lg2, and Tgfb1 loci in MEL cells.

(B) Percentage of Fli-1 binding regions in MEL cells located to promoter (1 kb upstream and downstream of the TSS, blue bars), intragenic (red bars), and intergenic (green bars) regions.

(C) Percentage of Fli-1 binding regions bound (blue bars) or not bound (yellow bars) by H3K4me1, H3K4me3, H3K9Ac, or H3K27Ac in MEL cells.

(D) List of the motifs enriched in the regions bound by Fli-1 in MEL cells (left panels) and their respective centrality compared with the FLI-1 peak (bottom panels).

(E) Proportion of Fli-1 bound regions containing the Fli-1 (blue bar) or the GATA1:TAL1 motif.

See also Figure S1 and Table S3.

Altogether, these data indicate that Fli-1 and the LDB1 complex mainly bind active enhancers in MEL cells, whereas Fli-1 without the LDB1 complex mainly bind active promoters.

FLI-1 enables the recruitment of the LDB1 complex to enhancers and tethers the interaction to the targeted promoter

The LDB1 complex is important for enhancer activity where it promotes chromatin looping with the associated promoter and the expression of the target genes (Soler et al., 2010; Stadhouders et al., 2012). However, except for the fusion protein EWS-FLI-1, the role of Fli-1 in these particular regions has not been addressed yet. To determine whether Fli-1 regulates the function of the LDB1 complex at enhancers regions, we focused on three regions in the *Meis1* locus bound by Fli-1 and the LDB1 complex, located at 94 (Meis1 +94), 55 (Meis1 +55), and 48 kb (Meis1 +48) downstream of the *Meis1* promoter (Figure 3A) and one region also bound by these proteins located 140 kb (Fut8-140) upstream of the *Fut8* promoter (Figure S2A). These genes were selected because of their known role in leukemia. In particular, *MEIS1* overexpression is

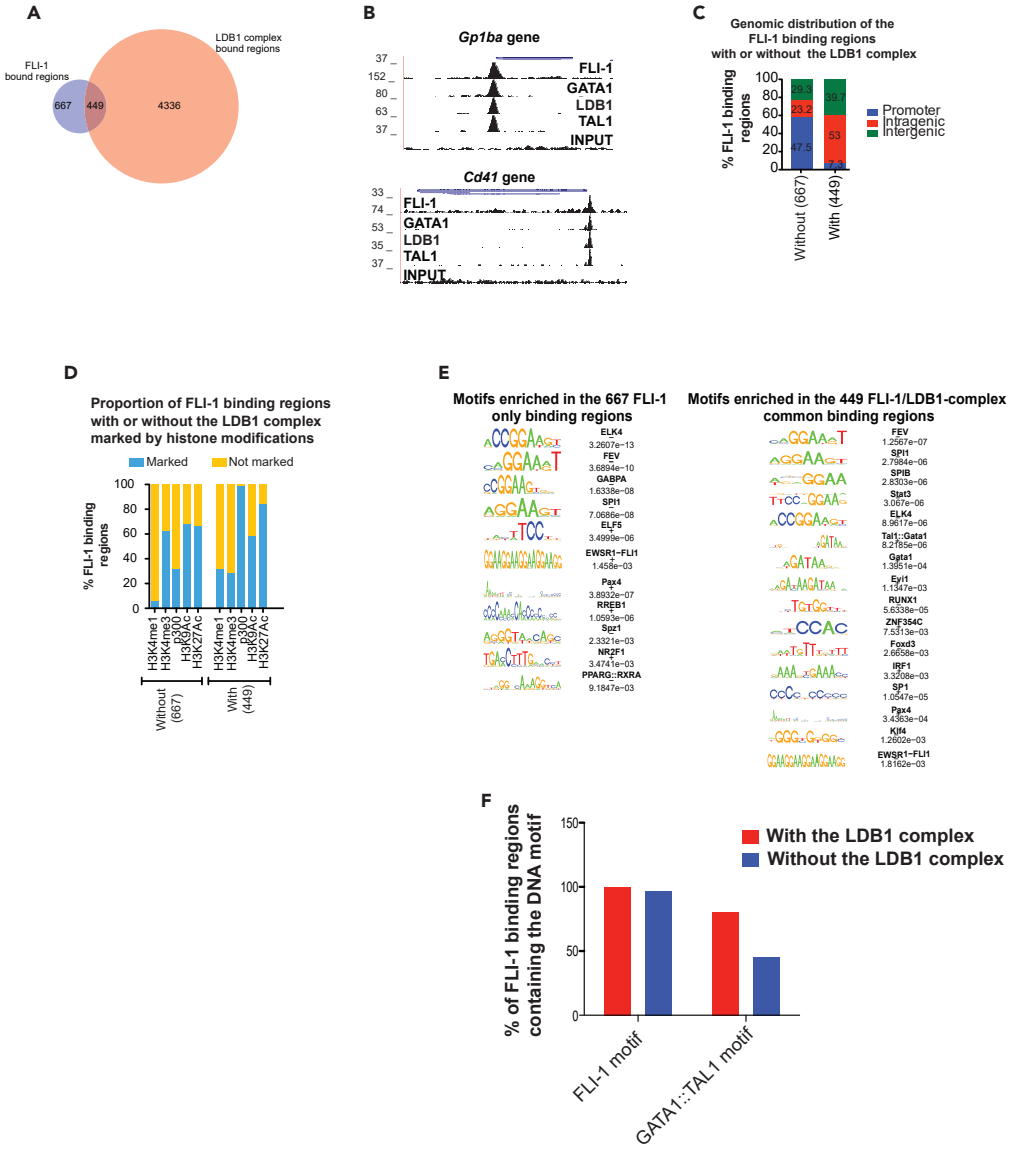

Figure 2. Fli-1 and the LDB1 complex mainly bind active enhancers in MEL cells

(A) Venn diagram displaying the overlap between the binding regions of Fli-1 (blue circle) and the LDB1 complex (red circle) in MEL cells.

(B) Genome view of the Fli-1, GATA1, LDB1, TAL1, and Input control ChIP-Seq data in MEL cells showing the co-recruitment of these proteins to the Gp1ba and Cd41 genes promoter.

(C) Percentage of Fli-1 binding regions with or without the LDB1 complex located to promoters (blue), intragenic (red), or intergenic (green) regions in MEL cells.

(D) Percentage of FLI-1 binding regions with or without the LDB1 complex marked (blue) or not marked (yellow) by H3K4me1, H3K4me3, P300, H3K9Ac, or H3K27Ac in MEL cells.

(E) List of the motifs enriched in the Fli-1 only binding regions (left panel) or in the common binding regions (right panel).

(F) Proportion of Fli-1 only (blue bars) or Fli-1/LDB1 complex commonly (red bars) bound regions containing the Fli-1 or the GATA1:TAL1 motif

See also Figure S1 and Table S3.

very often observed in acute myeloid leukemia and is associated with poor prognosis (Argiropoulos et al., 2007; Honma et al., 2015; Kumar et al., 2009; Liu et al., 2017; Wang et al., 2014). Besides, Sasaki et al. showed that FUT8 represses erythroid differentiation of MEL cells, as FLI-1 (Sasaki et al., 2013). Given the role of Fli-1 in erythroleukemia cells, the regulation of these two genes could be part of the molecular mechanisms

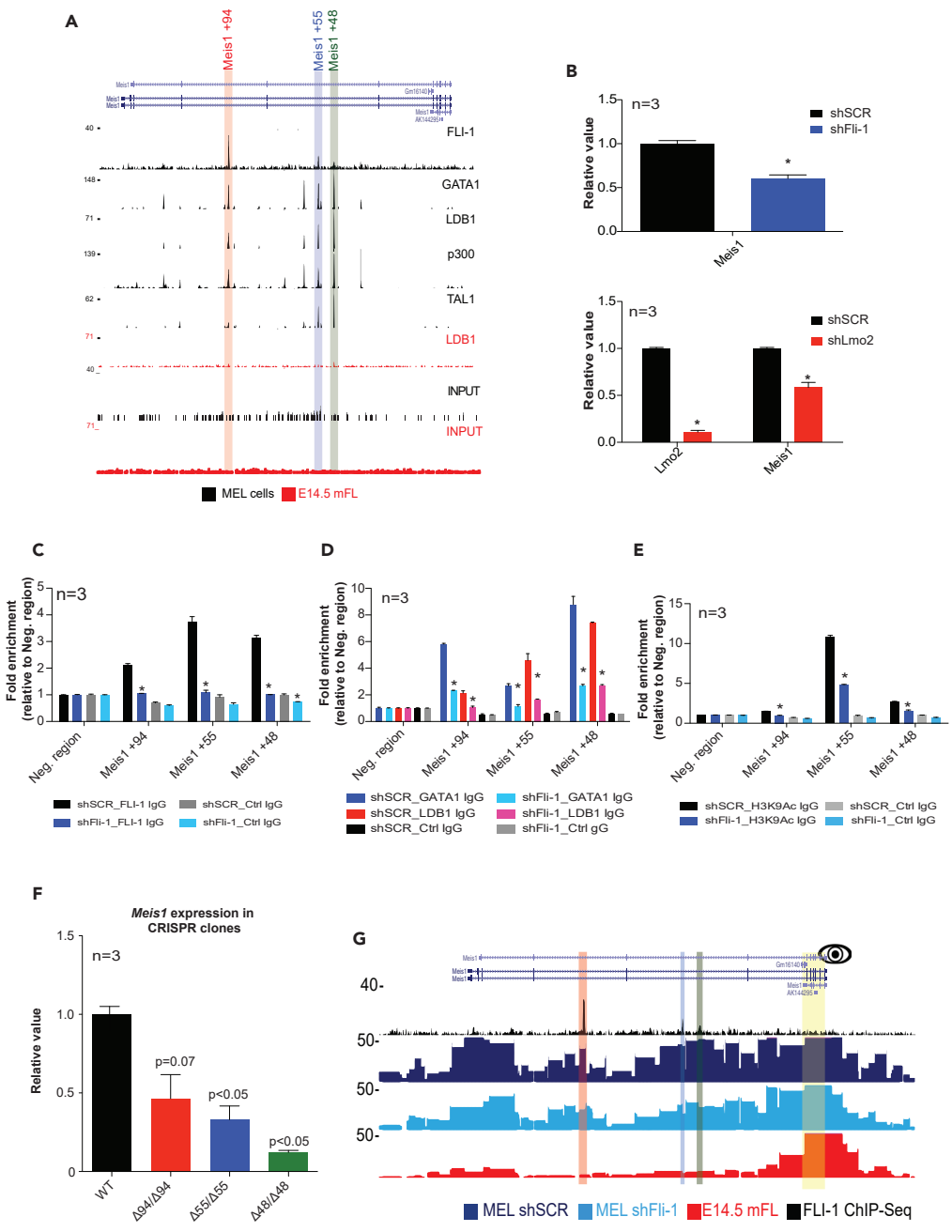

Figure 3. Fli-1 enables the recruitment of the LDB1 complex to 3 *Meis1* enhancers and promotes chromatin looping between these enhancers and the *Meis1* promoter in MEL cells

(A) ChIP-Seq profiles of Fli-1, TAL1, GATA1, and LDB1 in MEL cells (black) and in fetal liver cells (red) showing three binding regions located 94, 55, and 48 kb downstream of the Meis1 promoter.

(B) Top panel: Meis1 mRNA level from non-induced (dark color bars) and induced (light color bars) control (shSCR, black bars) or shFli-1 (blue bars) MEL cells. Bottom panel: Lmo2 and Meis1 mRNA level from control (shSCR, black bar) or shLmo2 transduced (red bar) MEL cells. The values are normalized to the value obtained for the Actb reference gene and those of control cells. Bars represent the geometric mean of three independent experiments. The error bars represent the standard error of the mean. *: $p < 0.05$ for the comparison between shSCR condition and the others (paired t test).

(C–E) Fli-1 (C), GATA1, LDB1 (D), and H3K9Ac (E) ChIP-qPCR experiments from control (shSCR, black) or shFli-1 (blue) MEL cells and primers amplifying the control Amylase region (Amy), the Meis1 +94, +55, and +48 regions. The bars represent the geometric mean of three replicates. The error bars represent the standard error of the mean. *: $p < 0.05$ for the comparison between shSCR condition and the others (paired t test).

Figure 3. *Continued*

(F) Meis1 mRNA levels from WT (black bar), Δ94/Δ94 (red bar), Δ55/Δ55 (blue bar), and Δ48/Δ48 (green bar) MEL cells. The values are normalized as in the panel c. The p values indicated above the bars have been obtained with a paired t test comparing WT MEL cells versus the Meis1 enhancer deleted CRISPR clones from three independent experiments.

(G) Fli-1 ChIP-Seq (black) and T2C profile of control (dark blue) or shFli-1 (light blue) MEL cells and E14.5 fetal liver cells (red) in the Meis1 locus. The Meis1 promoter is used as a viewpoint indicated by the eye symbol.

See also Figures S2 and S3.

triggered by Fli-1 to transform the erythroid lineage. Although Fli-1 is co-localized in these regions in MEL cells with the LDB1 complex, p300, and histone marks suggesting that these are potential enhancers of these genes, in mouse fetal livers, which contain erythroid progenitors and precursors, Fli-1 and the LDB1 complex are not recruited to these particular regions (Figures S2B and S2C). As expected, the lack of the recruitment of these proteins is correlated with a lower expression of *Meis1* and *Fut8* in mouse fetal liver cells when compared with MEL cells (Figures S2D and S2E). These observations suggest that Fli-1 enables the recruitment of the LDB1 complex to these particular enhancers contributing to the activation of their expression in MEL cells.

To test this hypothesis, we first performed RT-qPCR experiments after repression of either *Fli-1* or *Lmo2* (whose depletion prevents the recruitment of the LDB1 complex to DNA (Inoue et al., 2013)) in MEL cells and checked for the expression of *Meis1* and *Fut8*. As observed in Figures 3B and S2F, the repression of *Fli-1* and *Lmo2* triggers the decrease of *Meis1* and *Fut8* mRNA levels, indicating that Fli-1 and the LDB1 complex activate the expression of these two genes in MEL cells. Strikingly, ChIP-qPCR experiments show that *Fli-1* repression in MEL cells significantly decreases the recruitment of both GATA1 and LDB1 to *Meis1 +94*, *Meis1+55*, *Meis1+48*, and *Fut8-140* regions, whereas GATA1 and LDB1 protein levels remain stable when compared with control cells (Figures 3C, 3D, S2G, and S2H). These experiments suggest that Fli-1 enables the recruitment or the stabilization of the LDB1 complex to these regions in MEL cells.

Similar ChIP-qPCR experiments show that in MEL cells, these regions are more often characterized by the deposition of the active histone mark H3K9Ac than in mouse fetal liver cells (Figure S2I) and that the repression of *Fli-1* decreases the level of this histone mark at all these four regions in MEL cells (Figures 3E and S2J), indicating that FLI-1 is important to maintain the active chromatin state. In addition to the recruitment of the p300 acetyltransferase, these observations suggest that these four regions act as enhancers of the *Meis1* and *Fut8* gene. To confirm this hypothesis, we used CRISPR/Cas9 system (Cong et al., 2013; Ran et al., 2013) to homozygously delete *Meis1+94*, *Meis+55*, or *Meis1+48* in MEL cells (Figure S3A) and checked for the expression of *Meis1* in these MEL cells clones. As a result, *Meis1* expression is decreased in these three clones compared with wild-type MEL cells, demonstrating that these three regions are indeed *Meis1* enhancers (Figure 3F).

Enhancers regions activate gene expression through chromatin looping with the target promoter (Kolovos et al., 2012). Because the LDB1 complex promotes looping of the DNA (Soler et al., 2010; Stadhouders et al., 2012), we investigated whether the decrease of *Meis1* expression observed after *Fli-1* repression is correlated with a change of the 3D conformation of this locus. Therefore, we performed a T2C analysis focusing on the *Meis1* locus in control MEL cells, *Fli-1* repressed MEL cells, and mouse fetal liver cells (Kolovos et al, 2014, 2018). The overall architecture of the *Meis1* locus remains generally unchanged in FLI-1 depleted cells compared with wild-type MEL cells (with the exception of some changes in the local interactome), whereas we observe major differences (such as fewer interactions) in mouse fetal liver cells (Figure S3B). These observations agree with the level of *Meis1* expression in mouse fetal liver cells and in Fli-1 depleted MEL cells, where *Meis1* is either completely or partially repressed, respectively (Figures 3B and S2D). When the *Meis1* promoter is taken as a viewpoint, we observed that the three enhancer regions bound by Fli-1 and the LDB1 complex are in close proximity with the *Meis1* promoter (Figures 3G and S3C). In contrast, in mouse fetal liver cells, we do not observe an interaction with the *Meis1* enhancers. This indicates that in mouse fetal liver cells, *Meis1* promoter and enhancers are not in close proximity. Finally, the close proximity between the *Meis1* promoter and enhancers is retained, albeit at a lesser level, upon *Fli-1* repression (Figures 3G and S3C). The same observations can be made when one of the three enhancers is used as viewpoints (Figure S3D). We also checked the local interactome of the *Fut8* locus by performing 3C-Seq experiments in the same conditions (Stadhouders et al., 2013). These experiments highlight that the *Fut8-140* and *Fut8* promoter regions are also in close proximity in MEL cells and that this proximity depends on Fli-1 (Figures S3E and S3F). In mouse fetal liver cells, these two regions are also in

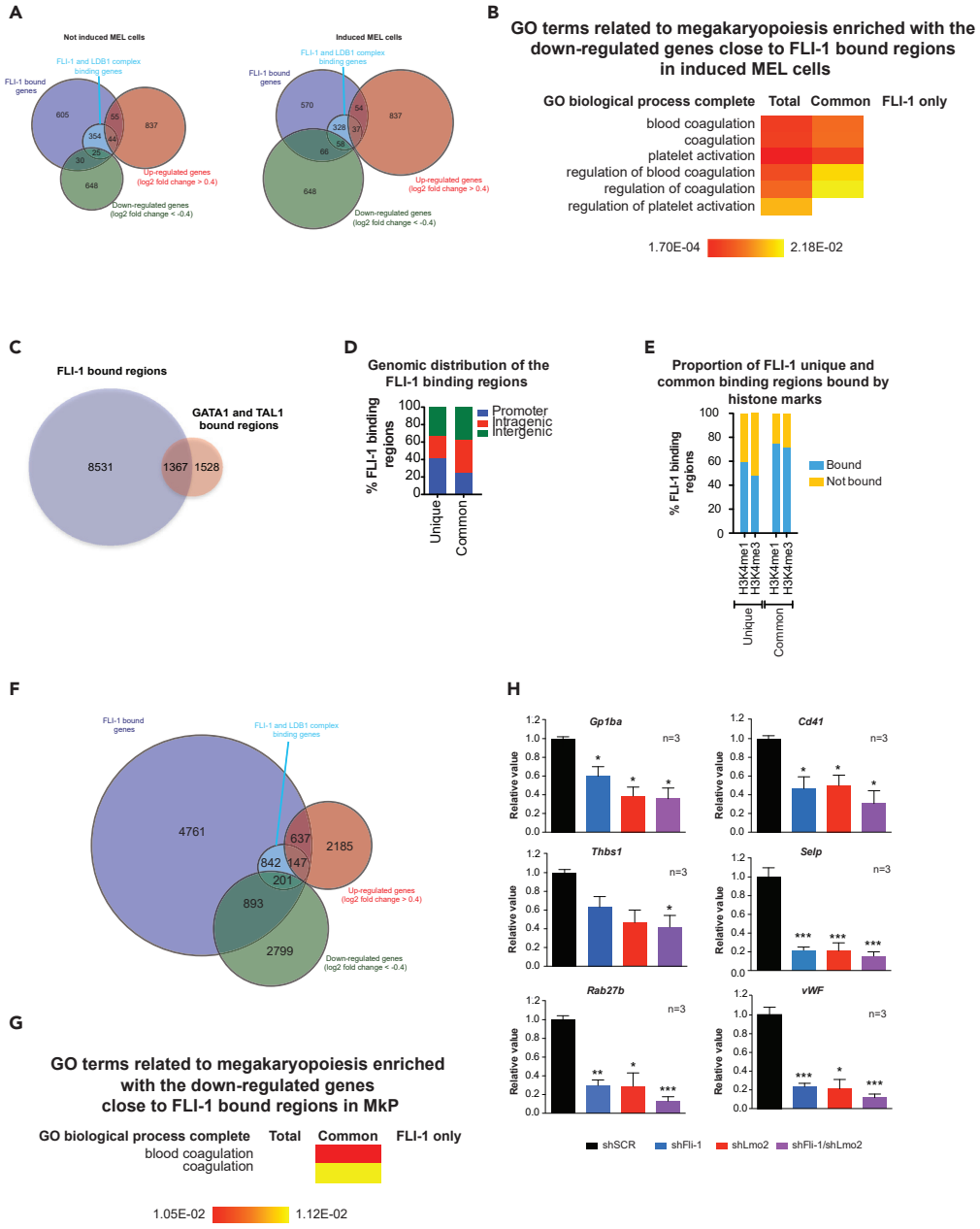

Figure 4. Fli-1 and the LDB1 complex activate megakaryocytic gene expression in MEL cells and megakaryocytes and promote megakaryopoiesis

(A) Venn diagram displaying the overlap between the list of genes near the Fli-1 binding regions (dark blue circle) or near the Fli-1 and LDB1 complex common binding regions (light blue circle) and the list of downregulated genes (green circle) or upregulated genes (red circle) after *Fli-1* repression in non-induced (left panel) or in induced MEL cells (right panel).

(B) GO terms relative to megakaryopoiesis enriched in the list of downregulated genes near FLI-1 binding regions in induced MEL cells

(C) Venn diagram displaying the overlap between the binding regions of Fli-1 (blue circle) and the LDB1 complex (GATA-1 and TAL1 red circle) in megakaryocytes.

(D) Percentage of Fli-1 binding regions with (common) or without (unique) the LDB1 complex located to promoters (blue), intragenic (red), or intergenic (green) regions in megakaryocytes.

(E) Percentage of Fli-1 binding regions with (common) or without (unique) the LDB1 complex bound (blue) or not bound (yellow) by H3K4me1 or H3K4me3 in megakaryocytes.

Figure 4. *Continued*
(F) Venn diagram showing the overlap between the genes close to Fli-1 binding regions (dark blue circle) or close to Fli-1 and LDB1 complex common binding regions (light blue circle) and the genes either downregulated (green circle) or upregulated (red circle) after Fli-1 repression in megakaryocytes.
(G) GO terms relative to megakaryopoiesis enriched in the list of downregulated genes near FLI-1 binding regions in MkP.
(H) Quantification of Gp1ba, Cd41, Thbs1, Selp, Rab27b, and vWF mRNA levels by RT-qPCR experiments from cells transduced with the shSCR (black bar), shFli-1 (blue bar), shLmo2 (red bar), or both (purple bar) lentiviruses. The bars represent the geometric mean of three independent experiments. The values are normalized to the value obtained in each condition for the Actb reference gene. The error bars represent the standard error of the mean. *: $p < 0.05$; **: $p < 0.01$; ***: $p < 0.005$ for the comparison between shSCR condition and the others (paired t test).
See also Figure S4 and Tables S4 and S5.

close proximity although at lower frequency compared with MEL cells, which correlate with *Fut8* expression in these two cell types.

Altogether, these data show that Fli-1 either enables the recruitment of the LDB1 complex or stabilizes this complex to enhancers commonly bound by these proteins. Moreover, Fli-1 is involved in their proximity with their target promoter through chromatin looping, and together, Fli-1 and the LDB1 complex activate the expression of these common target genes.

Fli-1 and the LDB1 complex directly activate the expression of megakaryocyte genes in MEL cells and promote megakaryopoiesis

We finally addressed the influence of the Fli-1 and LDB1 complex binding on gene expression. We performed RNA-Seq experiments in non-induced and DMSO-induced MEL cells after *Fli-1* repression and we crossed the list of deregulated genes (log2 fold change >0.4 or < −0.4) with the list of genes targeted by either FLI-1 alone or commonly by the Fli-1/LDB1 complex. Overall, the overlap is small, suggesting that other proteins such as PU.1 are compensating the absence of FLI-1 (Juban et al., 2009) (Figure 4A). As already shown in previous studies, gene ontology analyses using PANTHER (Tables S5 and S6) show that Fli-1 directly activates the expression of genes involved in ribosome biogenesis independently of the recruitment of the LDB1 complex. Interestingly, several terms related to megakaryocyte function (blood coagulation etc) are enriched in the list of downregulated genes targeted by the Fli-1/LDB1 complex in induced MEL cells (Figure 4B), suggesting that Fli-1 and the LDB1 complex activate the expression of megakaryocytic genes in an erythroleukemic context. To check whether Fli-1 is important for the recruitment of the LDB1 complex to the regulatory sequences of these genes, as previously observed at enhancer regions, we performed GATA1 and LDB1 ChIP-qPCR experiments in non-induced and induced MEL cells after *Fli-1* repression at the *Gp1ba* and *Cd41* promoter regions, 2 known genes involved in megakaryopoiesis. This shows they are decreased when *Fli-1* is repressed, indicating that Fli-1 also enables the recruitment of the LDB1 complex or stabilizes it to regulatory sequences of megakaryocytic genes in MEL cells (Figure S4A).

These data suggest that Fli-1 and the LDB1 complex are important for megakaryopoiesis. To test this hypothesis, we analyzed the Fli-1, GATA1, and TAL1 genome-wide bound regions in megakaryocytes (Pimkin et al., 2014; Yue et al., 2014). We crossed the Fli-1 binding regions with the regions bound by both GATA1 and TAL1 (considered as the LDB1 complex). The number of Fli-1 binding regions in megakaryocytes is much higher than in MEL cells, suggesting that the chromatin is more permissive for Fli-1 in megakaryocyte. One thousand three hundred sixty seven regions are bound by these three proteins and therefore by Fli-1 and the LDB1 complex (Figure 4C). We confirmed by ChIP-qPCR the recruitment of Fli-1, GATA1, and LDB1 on some regions in the L8057 megakaryoblastic cell line (Figures S4B and S4C). As in MEL cells, Fli-1 binding regions are less present in promoters when it is with the LDB1 complex than without (Figure 4D). Moreover, Fli-1/LDB1 complex commonly bound regions are more frequently marked by active histone modifications (H3K4me1 and H3K4me3) than regions bound by Fli-1 alone, indicating that Fli-1 binds preferentially active regions when it is with the LDB1 complex (Figure 4E). We then performed RNA-Seq experiments in megakaryocyte progenitors (MkP) isolated from wild-type or *Fli-1* KO mice (Figure S4D) and crossed the list of misregulated genes with the list of FLI-1 bound regions with or without the LDB1 complex (Pronk et al., 2007; Starck et al., 2010). As in MEL cells, the overlap is relatively small, most likely because of compensatory mechanisms (Figure 4F). We performed gene ontology analyses using PANTHER (Table S7). Again, we identified terms related to megakaryopoiesis in the list

of Fli-1/LDB1 complex commonly targeted genes, which are downregulated after *Fli-1* KO (Figure 4G), suggesting that Fli-1 and the LDB1 complex directly activate the expression of megakaryocytic genes and then contribute to megakaryopoiesis.

To test this hypothesis, we isolated cKit$^+$ cells from mouse fetal liver cells, cultured them for 5 days in presence of mSCF and mTpo upon infection with lentiviruses expressing control shRNA or shRNA directed against *Fli-1* or *Lmo2* mRNA to repress their expression. After 4 more days of culture in presence of mTpo only, we isolated RNA and performed RT-qPCR experiments to quantify the expression of genes involved in terminal megakaryocyte differentiation and that are bound by Fli-1 and the LDB1 complex except for *Thbs1* (Figures S4E and S4F) (Chen et al., 2007). As expected, *Fli-1* and *Lmo2* expression are decreased when cells are infected with the lentiviruses expressing the shRNA directed against their mRNA (Figure S4G). *Fli-1* expression is decreased as well when *Lmo2* is repressed, suggesting that the LDB1 complex regulates *Fli-1* expression in megakaryocytes. Finally, the expression of the genes, which are activated upon terminal megakaryocyte differentiation, are also decreased after *Fli-1* and *Lmo2* repression (Figure 4H). Finally, to check whether Fli-1 is important for the recruitment of the LDB1 complex on the promoters of *Gp1ba* and *Cd41* megakaryocytic genes as it is in MEL cells, we performed ChIP-qPCR experiment in mouse fetal liver cells cultured with SCF and mTPO cytokines and infected with the lentiviruses expressing either control shRNA or shRNA against *Fli-1* mRNA. We confirmed the recruitment of Fli-1, GATA1, and LDB1 to the promoter of these two megakaryocytic genes in control cells (Figure S4H). In *Fli-1*-repressed fetal liver cells, we observed a decreased binding of Fli-1, GATA1, and LDB1 to these two promoters, suggesting that, as in MEL cells, Fli-1 either stabilizes or enables the recruitment of the LDB1 complex to megakaryocytic gene regulatory sequences (Figure S4H). Interestingly, these two particular regions are also bound by Fli-1, GATA1, and TAL1 in human megakaryocytes, suggesting that the mode of regulation of megakaryocytic genes by Fli-1 and the LDB1 complex is conserved in human.

Altogether, these data show that Fli-1 and the LDB1 complex directly co-activate the expression of megakaryocytic genes both in MEL cells and in megakaryocyte and suggest that Fli-1 and the LDB1 complex cooperate to promote megakaryopoiesis.

DISCUSSION

The aim of this study is to bring new insights about the molecular mechanisms involved in the several Fli-1 contributions to physiological and pathological development, especially in combination with the LDB1 complex. We show here that Fli-1 and the LDB1 complex mainly bind active enhancers in MEL cells and directly activate the expression of megakaryocytic genes promoting terminal megakaryocyte differentiation.

Fli-1 enables the recruitment of the LDB1 complex both at enhancers and regulatory sequences of megakaryocytic genes (Figures 3C–3E, S2G, and S4A). However, how Fli-1 contributes to maintain the LDB1 complex bound to DNA remains elusive. One explanation would be that Fli-1 acts as a pioneer TF for the LDB1 complex at these common binding regions. These particular TFs are characterized by their ability to bind chromatin in a repressed state and to open it by recruiting cofactors. The decrease of the H3K9Ac level in these common binding enhancer regions when FLI-1 is repressed is in favor with such a role of Fli-1 in MEL cells. A similar role has been described for Fli-1 in AML-ETO acute myeloid leukemia cells where the AML-ETO oncoprotein is recruited to pre-occupied Fli-1 bound regions (Martens et al., 2012). Nevertheless, we cannot exclude that Fli-1 actually stabilizes the LDB1 complex when bound to DNA. Interestingly, STAT3 DNA motif is only enriched in the regions bound by both Fli-1 and the LDB1 complex. GATA1 and phosphorylated STAT3 interact in MEL and human K562 cells and are both bound to gamma globin gene (Yao et al., 2009). However, the activation of the JAK-STAT signaling by IL-6, which increases the binding of STAT3 to these regions, is associated with a decrease of GATA1 binding and gamma globin gene silencing. These data show that phosphorylated STAT3 inhibits the recruitment of GATA1 at least at the gamma globin locus. Strikingly, the STAT3 DNA motif contains the ETS DNA binding motif recognized by Fli-1, which would suggest that Fli-1 and STAT3 are in competition to be recruited to this particular motif. Therefore, we hypothesize that FLI-1 prevents the recruitment of STAT3 at Fli-1/LDB1 complex binding regions hence favoring the recruitment of the LDB1 complex. Activating or repressing the JAK-STAT signaling pathway would then influence the interaction and the co-recruitment of Fli-1 and the LDB1 complex. Post-translational modifications of members of

the LDB1 complex, especially of GATA1 have been shown to regulate their DNA-binding activity such as phosphorylation or acetylation (Lamonica et al., 2006; Partington and Patient, 1999). Another mechanism by which Fli-1 regulates the recruitment of the LDB1 complex to common binding regions would therefore be to recruit an enzyme that will modify the complex. Interestingly, the TRRAP acetyl-transferase appears in the top 10 of the Fli-1 protein partners identified by mass spectrometry (Giraud et al., 2014). TRRAP was already shown to interact with several TF and regulate their transcriptional activity (Liu et al., 2003). Whether TRRAP interacts with and acetylates GATA1 or another member of the LDB1 complex is still not known. Further experiments then have to be performed to decipher the potential contribution of TRRAP in the recruitment of the LDB1 complex.

We subsequently sought to investigate the role of Fli-1 in 3D chromatin conformation by studying two loci, *Meis1* and *Fut8* with three and one enhancer, respectively. We observed that the role of Fli-1 in 3D chromatin conformation, is loci dependent. The regulation of *Fut8* and promoter-enhancer interaction is dependent by the presence of FLI-1 (Figures S3A, S3F, and S3G). Notably, the promoter-enhancer interaction for *Meis1* appears to be stable and slightly affected by the binding of Fli-1 at its enhancers (Figures 3G and S3B–S3D). Therefore, we postulate that *Meis1* is stably in close proximity with its enhancers, potentially resembling a pre-looped conformation reported for other loci, where the promoter is continuously in close proximity with its enhancer, and only the presence of a TF (in this case Fli-1) activates the transcription of the gene (Kolovos et al., 2016). Therefore, most likely by enabling the recruitment of the LDB1 complex, which has a well-established role on those regions, Fli-1 promotes chromatin looping between the enhancers bound by both Fli-1 and the LDB1 complex and their target promoter. *Meis1* and *Fut8* gene, which are activated by Fli-1 and the LDB1 complex bound at their enhancer regions, encode two proteins, which have functions in different cancer. Indeed, *Meis1* aberrant expression actively contributes to acute myeloid leukemia, whereas *Fut8* overexpression has been found in non-hematopoietic cancer (Argiropoulos et al., 2007; Honma et al., 2015; Kumar et al., 2009; Liu et al., 2017; Wang et al., 2014). Besides, FUT8 inhibits erythroid differentiation of MEL cells and K562 cells, which suggests that FUT8 also contributes to erythroleukemia (Sasaki et al., 2013). Therefore, targeting enhancers of genes involved in leukemia would be one mechanism by which Fli-1 contributes to erythroleukemia. In addition to bringing new insights concerning Fli-1 contributions to cancer, our data identify three new enhancers of *Meis1* in erythroleukemia. As mentioned earlier, *Meis1* expression promotes leukemia development. Nevertheless, it is still unclear how *Meis1* is overexpressed in such pathological condition. Testing whether Fli-1 and the LDB1 complex co-regulate *MEIS1* in this context would be interesting for therapeutic purpose.

Finally, we showed that Fli-1 and the LDB1 complex directly activate the expression of megakaryocytic genes both in MEL cells and in megakaryocytes and promote terminal megakaryocyte differentiation (Figures 4 and S5). The activation of genes involved in megakaryopoiesis in an erythroleukemic context supposes that MEL cells have an increased plasticity. This increased plasticity has been found as well in mice overexpressing another ETS TF, ERG, whose ETS DNA-binding domain has 98% homology with the one of Fli-1. These mice develop among other type of leukemia, acute erythroleukemia. When plated in methylcellulose with the appropriate cytokines, these erythroleukemic cells give rise to megakaryocytic colonies, showing that these cells kept the ability to express the megakaryocytic program (Carmichael et al., 2012). Whether keeping the megakaryocytic potentiality is a common feature in human acute erythroleukemia (AML-M6) has never been addressed yet. But we think that first checking whether AML-M6 cells still express megakaryocytic genes and developing strategies to repress it would improve the current therapies against such leukemia. Next to being co-recruited in terminally differentiated cells, Fli-1 and the LDB1 complex share already common binding regions in immature progenitor cells such as hemogenic endothelium and multipotent hematopoietic progenitors, suggesting that they also interplay at early stages of hematopoiesis. Recently, hematopoietic stem cells with a megakaryocytic bias have been identified (Shin et al., 2014). Whether Fli-1 and the LDB1 complex play a role in these HSC have not been addressed yet, but seeing our data and the aforementioned data, we suspect that these proteins are involved in priming those cells toward megakaryocytes. As already mentioned, a cocktail composed of Fli-1, GATA1, and TAL1 have been used to enhance megakaryocyte production (Moreau et al., 2016). We propose to improve this strategy by adding both LDB1 and LMO2.

Limitations of the study

The results in this study are obtained in murine transformed cell lines or mouse primary cells. Although the FLI-1 and the LDB1 complex binding sites shown in this study seem to be conserved in humans, the data

presented in this work might not entirely reflect what happens in humans. Therefore, tackling the interplay between FLI-1 and the LDB1 complex in human primary cells will definitely validate its role in leukemia and megakaryopoiesis.

Resource availability

Lead contact

Dr Guillaume GIRAUD—guillaume.giraud@inserm.fr.

Materials availability

The study did not generate new unique reagents.

Data and code availability

The accession number for the FLI-1 ChIP-Seq, the RNA-Seq and the T2C experiments reported in this paper is SRA: SRP158024.

METHODS

All methods can be found in the accompanying transparent methods supplemental file.

SUPPLEMENTAL INFORMATION

Supplemental information can be found online at https://doi.org/10.1016/j.isci.2021.102210.

ACKNOWLEDGMENTS

The authors acknowledge all the members of the Cell Biology Department at the Erasmus Medical Center for fruitful discussion. The authors acknowledge the members of the Biomics Department at the Erasmus Medical Center for the sequencing data. The authors also acknowledge the members of the animal house facility at the Erasmus Medical Center for taking care of the mice. This work was supported by the EU grants Syboss (GG) and Thalamos (PK) and a BIG grant (Erasmus MC) to FG.

AUTHOR CONTRIBUTIONS

Conceptualization, G.G. and F.G.; Methodology, G.G., P.K., F.G., I.B.; Software, P.K.; Validation, G.G. and I.B.; Formal Analysis, G.G., P.K., I.B., J.v.S., M.W.G, and B.G., Investigation, G.G. and I.B.; Resources, G.G. and F.G.; Data Curation, G.G. and F.G.; Writing—Original draft, G.G.; Writing—Review & Editing, F.G., P.K., and I.B.; Visualization, G.G. and I.B., Supervision, G.G. and F.G., Project Administration; G.G. and F.G.; Funding Acquisition, F.G.

DECLARATION OF INTERESTS

The authors declare no competing of interest.

Received: October 10, 2019
Revised: December 22, 2020
Accepted: February 17, 2021
Published: March 19, 2021

REFERENCES

Argiropoulos, B., Yung, E., and Humphries, R.K. (2007). Unraveling the crucial roles of Meis1 in leukemogenesis and normal hematopoiesis. Genes Dev. *21*, 2845–2849.

Ben-David, Y., Giddens, E.B., and Bernstein, A. (1990). Identification and mapping of a common proviral integration site Fli-1 in erythroleukemia cells induced by Friend murine leukemia virus. Proc. Natl. Acad. Sci. U S A *87*, 1332–1336.

Ben-David, Y., Giddens, E.B., Letwin, K., and Bernstein, A. (1991). Erythroleukemia induction by Friend murine leukemia virus: insertional activation of a new member of the ets gene family, Fli-1, closely linked to c-ets-1. Genes Dev. *5*, 908–918.

Bhagwat, A.S., and Vakoc, C.R. (2015). Targeting transcription factors in cancer. Trends Cancer *1*, 53–65.

Carmichael, C.L., Metcalf, D., Henley, K.J., Kruse, E.A., Di Rago, L., Mifsud, S., Alexander, W.S., and Kile, B.T. (2012). Hematopoietic overexpression of the transcription factor Erg induces lymphoid and erythro-megakaryocytic leukemia. Proc. Natl. Acad. Sci. U S A *109*, 15437–15442.

Chen, Z., Hu, M., and Shivdasani, R.A. (2007). Expression analysis of primary mouse megakaryocyte differentiation and its application in identifying stage-specific molecular markers and a novel transcriptional target of NF-E2. Blood *109*, 1451–1459.

Cong, L., Ran, F.A., Cox, D., Lin, S., Barretto, R., Habib, N., Hsu, P.D., Wu, X., Jiang, W., Marraffini, L.A., and Zhang, F. (2013). Multiplex genome

engineering using CRISPR/Cas systems. Science *339*, 819–823.

Giraud, G., Stadhouders, R., Conidi, A., Dekkers, D.H.W., Huylebroeck, D., Demmers, J.A.A., Soler, E., and Grosveld, F.G. (2014). NLS-tagging: an alternative strategy to tag nuclear proteins. Nucleic Acids Res. *42*, e163.

Hamlett, I., Draper, J., Strouboulis, J., Iborra, F., Porcher, C., and Vyas, P. (2008). Characterization of megakaryocyte GATA1-interacting proteins: the corepressor ETO2 and GATA1 interact to regulate terminal megakaryocyte maturation. Blood *112*, 2738–2749.

Honma, R., Kinoshita, I., Miyoshi, E., Tomaru, U., Matsuno, Y., Shimizu, Y., Takeuchi, S., Kobayashi, Y., Kaga, K., Taniguchi, N., and Dosaka-Akita, H. (2015). Expression of fucosyltransferase 8 is associated with an unfavorable clinical outcome in non-small cell lung cancers. Oncology *88*, 298–308.

Inoue, A., Fujiwara, T., Okitsu, Y., Katsuoka, Y., Fukuhara, N., Onishi, Y., Ishizawa, K., and Harigae, H. (2013). Elucidation of the role of LMO2 in human erythroid cells. Exp. Hematol. *41*, 1062–1076.e1.

Juban, G., Giraud, G., Guyot, B., Belin, S., Diaz, J.-J., Starck, J., Guillouf, C., Moreau-Gachelin, F., and Morlé, F. (2009). Spi-1 and Fli-1 directly activate common target genes involved in ribosome biogenesis in Friend erythroleukemic cells. Mol. Cell Biol. *29*, 2852–2864.

Kawada, H., Ito, T., Pharr, P.N., Spyropoulos, D.D., Watson, D.K., and Ogawa, M. (2001). Defective megakaryopoiesis and abnormal erythroid development in Fli-1 gene-targeted mice. Int. J. Hematol. *73*, 463–468.

Kolovos, P., Brouwer, R.W.W., Kockx, C.E.M., Lesnussa, M., Kepper, N., Zuin, J., Imam, A.M.A., van de Werken, H.J.G., Wendt, K.S., Knoch, T.A., et al. (2018). Investigation of the spatial structure and interactions of the genome at sub-kilobase-pair resolution using T2C. Nat. Protoc. *13*, 459–477.

Kolovos, P., Georgomanolis, T., Koeferle, A., Larkin, J.D., Brant, L., Nikolicć, M., Gusmao, E.G., Zirkel, A., Knoch, T.A., van Ijcken, W.F., et al. (2016). Binding of nuclear factor κB to noncanonical consensus sites reveals its multimodal role during the early inflammatory response. Genome Res. *26*, 1478–1489.

Kolovos, P., Knoch, T.A., Grosveld, F.G., Cook, P.R., and Papantonis, A. (2012). Enhancers and silencers: an integrated and simple model for their function. Epigenetics Chromatin *5*, 1.

Kolovos, P., van de Werken, H.J., Kepper, N., Zuin, J., Brouwer, R.W., Kockx, C.E., Wendt, K.S., van IJcken, W.F., Grosveld, F., and Knoch, T.A. (2014). Targeted Chromatin Capture (T2C): a novel high resolution high throughput method to detect genomic interactions and regulatory elements. Epigenetics Chromatin *7*, 10.

Kornblau, S.M., Qiu, Y.H., Zhang, N., Singh, N., Faderl, S., Ferrajoli, A., York, H., Qutub, A.A., Coombes, K.R., and Watson, D.K. (2011). Abnormal expression of FLI1 protein is an adverse prognostic factor in acute myeloid leukemia. Blood *118*, 5604–5612.

Krivega, I., Dale, R.K., and Dean, A. (2014). Role of LDB1 in the transition from chromatin looping to transcription activation. Genes Dev. *28*, 1278–1290.

Krivega, I., and Dean, A. (2017). LDB1-mediated enhancer looping can be established independent of mediator and cohesin. Nucleic Acids Res. *45*, 8255–8268.

Kumar, A.R., Li, Q., Hudson, W.A., Chen, W., Sam, T., Yao, Q., Lund, E.A., Wu, B., Kowal, B.J., and Kersey, J.H. (2009). A role for MEIS1 in MLL-fusion gene leukemia. Blood *113*, 1756–1758.

Lamonica, J.M., Vakoc, C.R., and Blobel, G.A. (2006). Acetylation of GATA-1 is required for chromatin occupancy. Blood *108*, 3736–3738.

Lee, J., Krivega, I., Dale, R.K., and Dean, A. (2017). The LDB1 complex Co-opts CTCF for erythroid lineage-specific long-range enhancer interactions. Cell Rep. *19*, 2490–2502.

Li, L., Freudenberg, J., Cui, K., Dale, R., Song, S.-H., Dean, A., Zhao, K., Jothi, R., and Love, P.E. (2013). Ldb1-nucleated transcription complexes function as primary mediators of global erythroid gene activation. Blood *121*, 4575–4585.

Liu, J., Qin, Y.-Z., Yang, S., Wang, Y., Chang, Y.-J., Zhao, T., Jiang, Q., and Huang, X.-J. (2017). Meis1 is critical to the maintenance of human acute myeloid leukemia cells independent of MLL rearrangements. Ann. Hematol. *96*, 567–574.

Liu, X., Tesfai, J., Evrard, Y.A., Dent, S.Y.R., and Martinez, E. (2003). c-Myc transformation domain recruits the human STAGA complex and requires TRRAP and GCN5 acetylase activity for transcription activation. J. Biol. Chem. *278*, 20405–20412.

Love, P.E., Warzecha, C., and Li, L. (2014). Ldb1 complexes: the new master regulators of erythroid gene transcription. Trends Genet. *30*, 1–9.

Martens, J.H.A., Mandoli, A., Simmer, F., Wierenga, B.-J., Saeed, S., Singh, A.A., Altucci, L., Vellenga, E., and Stunnenberg, H.G. (2012). ERG and FLI1 binding sites demarcate targets for aberrant epigenetic regulation by AML1-ETO in acute myeloid leukemia. Blood *120*, 4038–4048.

Masuya, M., Moussa, O., Abe, T., Deguchi, T., Higuchi, T., Ebihara, Y., Spyropoulos, D.D., Watson, D.K., and Ogawa, M. (2005). Dysregulation of granulocyte, erythrocyte, and NK cell lineages in Fli-1 gene-targeted mice. Blood *105*, 95–102.

Moreau, T., Evans, A.L., Vasquez, L., Tijssen, M.R., Yan, Y., Trotter, M.W., Howard, D., Colzani, M., Arumugam, M., Wu, W.H., et al. (2016). Large-scale production of megakaryocytes from human pluripotent stem cells by chemically defined forward programming. Nat. Commun. *7*, 11208.

Moussa, O., LaRue, A.C., Abangan, R.S., Williams, C.R., Zhang, X.K., Masuya, M., Gong, Y.Z., Spyropoulos, D.D., Ogawa, M., Gilkeson, G., and Watson, D.K. (2010). Thrombocytopenia in mice lacking the carboxy-terminal regulatory domain of the Ets transcription factor Fli1. Mol. Cell Biol. *30*, 5194–5206.

Nebert, D.W. (2002). Transcription factors and cancer: an overview. Toxicology *181–182*, 131–141.

Partington, G.A., and Patient, R.K. (1999). Phosphorylation of GATA-1 increases its DNA-binding affinity and is correlated with induction of human K562 erythroleukaemia cells. Nucleic Acids Res. *27*, 1168–1175.

Pimkin, M., Kossenkov, A.V., Mishra, T., Morrissey, C.S., Wu, W., Keller, C.A., Blobel, G.A., Lee, D., Beer, M.A., Hardison, R.C., and Weiss, M.J. (2014). Divergent functions of hematopoietic transcription factors in lineage priming and differentiation during erythro-megakaryopoiesis. Genome Res. *24*, 1932–1944.

Pronk, C.J.H., Rossi, D.J., Månsson, R., Attema, J.L., Norddahl, G.L., Chan, C.K.F., Sigvardsson, M., Weissman, I.L., and Bryder, D. (2007). Elucidation of the phenotypic, functional, and molecular topography of a myeloerythroid progenitor cell hierarchy. Cell Stem Cell *1*, 428–442.

Ran, F.A., Hsu, P.D., Wright, J., Agarwala, V., Scott, D.A., and Zhang, F. (2013). Genome engineering using the CRISPR-Cas9 system. Nat. Protoc. *8*, 2281–2308.

Rapino, F., Robles, E.F., Richter-Larrea, J.A., Kallin, E.M., Martinez-Climent, J.A., and Graf, T. (2013). C/EBPα induces highly efficient macrophage transdifferentiation of B lymphoma and leukemia cell lines and impairs their tumorigenicity. Cell Rep *3*, 1153–1163.

Sasaki, H., Toda, T., Furukawa, T., Mawatari, Y., Takaesu, R., Shimizu, M., Wada, R., Kato, D., Utsugi, T., Ohtsu, M., and Murakami, Y. (2013). α-1,6-Fucosyltransferase (FUT8) inhibits hemoglobin production during differentiation of murine and K562 human erythroleukemia cells. J. Biol. Chem. *288*, 16839–16847.

Shin, J.Y., Hu, W., Naramura, M., and Park, C.Y. (2014). High c-Kit expression identifies hematopoietic stem cells with impaired self-renewal and megakaryocytic bias. J. Exp. Med. *211*, 217–231.

Soler, E., Andrieu-Soler, C., de Boer, E., Bryne, J.C., Thongjuea, S., Stadhouders, R., Palstra, R.-J., Stevens, M., Kockx, C., van Ijcken, W., et al. (2010). The genome-wide dynamics of the binding of Ldb1 complexes during erythroid differentiation. Genes Dev. *24*, 277–289.

Spyropoulos, D.D., Pharr, P.N., Lavenburg, K.R., Jackers, P., Papas, T.S., Ogawa, M., and Watson, D.K. (2000). Hemorrhage, impaired hematopoiesis, and lethality in mouse embryos carrying a targeted disruption of the Fli1 transcription factor. Mol. Cell Biol *20*, 5643–5652.

Stadhouders, R., Aktuna, S., Thongjuea, S., Aghajanirefah, A., Pourfarzad, F., van Ijcken, W., Lenhard, B., Rooks, H., Best, S., Menzel, S., et al. (2014). HBS1L-MYB intergenic variants modulate fetal hemoglobin via long-range MYB enhancers. J. Clin. Invest. *124*, 1699–1710.

Stadhouders, R., Kolovos, P., Brouwer, R., Zuin, J., van den Heuvel, A., Kockx, C., Palstra, R.-J., Wendt, K.S., Grosveld, F., van Ijcken, W., and Soler, E. (2013). Multiplexed chromosome conformation capture sequencing for rapid genome-scale high-resolution detection of long-

range chromatin interactions. Nat. Protoc. *8*, 509–524.

Stadhouders, R., Thongjuea, S., Andrieu-Soler, C., Palstra, R.-J., Bryne, J.C., van den Heuvel, A., Stevens, M., de Boer, E., Kockx, C., van der Sloot, A., et al. (2012). Dynamic long-range chromatin interactions control Myb proto-oncogene transcription during erythroid development. EMBO J. *31*, 986–999.

Starck, J., Weiss-Gayet, M., Gonnet, C., Guyot, B., Vicat, J.-M., and Morlé, F. (2010). Inducible Fli-1 gene deletion in adult mice modifies several myeloid lineage commitment decisions and accelerates proliferation arrest and terminal erythrocytic differentiation. Blood *116*, 4795–4805.

Suzuki, E., Karam, E., Williams, S., Watson, D.K., Gilkeson, G., and Zhang, X.K. (2012). Fli-1 transcription factor affects glomerulonephritis development by regulating expression of monocyte chemoattractant protein-1 in endothelial cells in the kidney. Clin. Immunol. *145*, 201–208.

Takahashi, K., and Yamanaka, S. (2006). Induction of pluripotent stem cells from mouse embryonic and adult fibroblast cultures by defined factors. Cell *126*, 663–676.

Wang, M., Wang, J., Kong, X., Chen, H., Wang, Y., Qin, M., Lin, Y., Chen, H., Xu, J., Hong, J., et al. (2014). MiR-198 represses tumor growth and metastasis in colorectal cancer by targeting fucosyl transferase 8. Sci. Rep. *4*, 6145.

Wei, G.-H., Badis, G., Berger, M.F., Kivioja, T., Palin, K., Enge, M., Bonke, M., Jolma, A., Varjosalo, M., Gehrke, A.R., et al. (2010). Genome-wide analysis of ETS-family DNA-binding in vitro and in vivo. EMBO J. *29*, 2147–2160.

Wilson, N.K., Foster, S.D., Wang, X., Knezevic, K., Schütte, J., Kaimakis, P., Chilarska, P.M., Kinston, S., Ouwehand, W.H., Dzierzak, E., et al. (2010). Combinatorial transcriptional control in blood stem/progenitor cells: genome-wide analysis of ten major transcriptional regulators. Cell Stem Cell *7*, 532–544.

Yan, X., Yu, Y., Li, L., Chen, N., Song, W., He, H., Dong, J., Liu, X., and Cui, J. (2018). Friend leukemia virus integration 1 is a predictor of poor prognosis of breast cancer and promotes metastasis and cancer stem cell properties of breast cancer cells. Cancer Med. *7*, 3548–3560.

Yao, X., Kodeboyina, S., Liu, L., Dzandu, J., Sangerman, J., Ofori-Acquah, S.F., and Pace, B.S. (2009). Role of STAT3 and GATA-1 interactions in gamma-globin gene expression. Exp. Hematol. *37*, 889–900.

Yue, F., Cheng, Y., Breschi, A., Vierstra, J., Wu, W., Ryba, T., Sandstrom, R., Ma, Z., Davis, C., Pope, B.D., et al. (2014). A comparative encyclopedia of DNA elements in the mouse genome. Nature *515*, 355–364.

iScience, Volume *24*

Supplemental information

Interplay between FLI-1 and the LDB1 complex in murine erythroleukemia cells and during megakaryopoiesis

Guillaume Giraud, Petros Kolovos, Ilias Boltsis, Jente van Staalduinen, Boris Guyot, Michele Weiss-Gayet, Wilfred van IJcken, François Morlé, and Frank Grosveld

SUPPLEMENTAL FIGURE LEGEND

Figure S1 (Related to Figure 1 and Figure 2) : FLI-1 and the LDB1 complex are co-recruited in MEL cells

a ChIP experiments performed with either the anti-FLI-1 antibody or the control IgG in non induced or induced MEL cells expressing either control shRNA (shSCR) or shRNA against the Fli-1 mRNA (shFli-1) followed by qPCR to amplify the control region in the β-amylase locus (Amy, black bar) or the FLI-1 binding regions identified by ChIP-Seq (see Figure 1d) in the Gp1ba (blue bar) and the Cd41 promoter (red bar) and in the Tgfb1 (green bar), Stat1 (orange bar), Trp53 (purple bar) and Pdcd1lg2 yellow bar) loci. The bars represent the geometric mean of the ratio between the FLI-1 binding regions and the control region of 3 independent experiments. The error bars represent the standard errors. *: $p<0.05$ for the comparison between shSCR and shFli-1 conditions (paired t-test).

b Western blot analyses of the FLI-1 (bottom blot) or the VCP (top blot, loading control) protein levels in non-induced (lanes 1 and 2) and induced (lanes 3 and 4) MEL cells expressing the control shRNA (shSCR, lanes 1 and 3) or the shRNA against Fli-1 mRNA (shFli-1, lanes 2 and 4). The blots are representative of 3 independent experiments.

c RT-qPCR analyses of the Fli-1 mRNA levels in non-induced and induced MEL cells expressing the control shRNA (shSCR, black bars) or the shRNA against Fli-1 mRNA (shFli-1, blue bars). The bars represent the geometric mean of the ratio of the signals between shFli-1 and shSCR normalized to the signals of the Actb reference gene of 3 independent experiments. The error bars represent the standard errors. *: $p<0.05$ for the comparison between shSCR and shFli-1 conditions (paired t-test).

d ChIP experiments performed with either the anti-GATA1 or the anti-LDB1 antibodies or the control IgG in non induced or induced MEL cells followed by qPCR to amplify the control region in the β-amylase locus (Amy, black bar) or the FLI-1 binding regions identified by ChIP-Seq (see Figure 1d) in the Gp1ba (blue bar) and the Cd41 promoter (red bar). The bars represent the geometric mean of the ratio between the FLI-1 binding regions and the control region of 3 independent experiments. The error bars represent the standard error.

Figure S2 (Related to Figure 3) : FLI-1 and the LDB1 complex directly activate *Fut8* and *Meis1* expression by binding to enhancers in MEL cells

a ChIP-Seq profiles of FLI-1, GATA1, LDB1, TAL1, LMO2, p300 and the Input control in MEL cells (black) and LDB1 and Input control in E14.5 mFL (red) on the Fut8 locus.

b ChIP experiments with the anti-FLI-1 (top panel), anti-GATA1 and anti-LDB1 (bottom panel) antibodies and their respective control IgG in MEL cells and E14.5 fetal liver cells (mFL) followed by qPCR experiments to amplify the amylase control region (Amy, black bar), the Meis1 +94 (red bar), the Meis1 +55 (blue bars) or the Meis1 +48 (green bars) regions. The bars represent the geometric mean of the ratio between the FLI-1 binding regions and the control region of 3 independent experiments. The error bars represent the standard error. *: $p<0.05$ for the comparison between MEL cells and fetal liver cells.

c ChIP-qPCR experiments performed with either an anti-FLI-1 (top panel), an anti-GATA1 or an anti-LDB1 (bottom panel) antibody and their respective control IgG in MEL cells and E14.5 mFL followed by qPCR amplifying the control Amylase region (black bars) and the Fut8-140 region (blue bar). The bars represent the geometric mean of the ratio between the FLI-1 binding regions and the control region of 3 independent experiments. The error bars represent the standard error. *: $p<0.05$ for the comparison between MEL cells and fetal liver cells.

d Quantification of the Meis1 mRNA levels by RT-qPCR experiments in E14.5 fetal liver (red bar) and MEL (blue bar) cells. The bars represent the geometric mean of the ratio between MEL cells and fetal liver cells. The error bars represent the standard error. *: $p<0.05$ for the comparison between MEL cells and fetal liver cells.

e Quantification of the Fut8 mRNA levels by RT-qPCR experiments in E14.5 fetal liver (red bar) and MEL (blue bar) cells. The bars represent the geometric mean of the ratio between MEL cells and fetal liver cells. The error bars represent the standard errors. *: $p<0.05$ for the comparison between MEL cells and fetal liver cells.

f Left panel: Fut8 mRNA level from non-induced control (shSCR, black bars) or shFli-1 (blue bars) MEL cells. Right panel: Lmo2 and Meis1 mRNA level from control (shSCR, black bar) or shLmo2 transduced (green bar) MEL cells. The values are normalized to the value obtained for the Actb reference gene and those of control cells. Bars represent the geometric mean of 3 independent experiments. The error bars represent the standard errors. *: $p<0.05$ for the comparison between shSCR condition and the others (paired t-test).

g ChIP-qPCR experiments using an anti-FLI-1 (top panel), an anti-LDB1 (middle panel) or an anti-

GATA1 (bottom panel) antibody and their respective control IgG in non –induced and induced control (shSCR) or shFli-1 MEL cells followed by qPCR amplifying the control Amylase region (black bars) and the Fut8-140 region (blue bar). The bars represent the average of the ratio between the FLI-1 binding regions and the control region of 3 independent experiments. The error bars represent the standard error. *: $p<0.05$ for the comparison between shSCR and shFli-1 conditions (paired t-test).
h Western blot analyses of GATA1 (2^{nd} top panel), LDB1 (bottom panel) VCP (loading control, top panel and 2^{nd} bottom panel) protein levels in non-induced (lanes 1 and 2) and induced (lanes 3 and 4) MEL cells expressing the control shSCR (lanes 1 and 3) or shFli-1 (lanes 2 and 4). The pictures are representative of 3 independent experiments.
i Left panel : ChIP experiment using an anti-H3K9Ac antibody or its control IgG from MEL cells or E14.5 mouse fetal liver cells followed by qPCR experiments to amplify the *Meis1+94* (red bars), the *Meis1+55* (blue bars) or the *Meis1+48* (green bars) regions. Right panel : ChIP experiment using an anti-H3K9Ac antibody or its control IgG from MEL cells or E14.5 mouse fetal liver cells followed by qPCR experiments to amplify the negative region (Amy, black bars) or the *Fut8-140* (blue bars) region. In the two panels, the bars represent the average of the relative value compared to Input of 3 independent experiments. The error bars represent the standard error. *: $p<0.05$ for the comparison between MEL cells and fetal liver cells.
j ChIP-qPCR experiments performed with an anti-H3K9Ac or its respective control IgG in control (shSCR) or shFli-1 non-induced or induced MEL cells followed by qPCR amplifying the control Amylase region (black bars) and the Fut8-140 region (blue bar). The bars represent the average of the relative value compared to Input of 3 independent experiments. The error bars represent the standard error. *: $p<0.05$ for the comparison between control and shFli-1 cells.

Figure S3 (Related to Figure 3) : FLI-1 and the LDB1 complex reshape the 3D chromatin landscape of *Meis1* and *Fut8* loci.
a Left panel: Scheme of the Meis1 locus. The promoter and the sense of transcription is indicated by an arrow. The Meis1 +48, Meis1 +55 and the Meis1 +94 regions are indicated by a green, blue and red rectangle respectively. The gRNA used to delete these 3 regions individually are indicated by scissors and the primers couple used to screen for clones having the deletion of the Meis1 +48, Meis1 +55 and the Meis1 +94 regions are indicated by
green, blue and red lanes respectively. Right panel: PCR using the primer couples mentioned above from gDNA of WT, Δ94/Δ94, Δ55/Δ55 and Δ48/Δ48 clones.
b T2C profiles on the Meis1 locus from MEL cells expressing either control shRNA (shSCR, middle panel) or shRNA targeting Fli-1 mRNA (shFli-1, top panel) or from mouse fetal liver cells (E14.5 mFL, bottom panel). Below are plotted the LDB1, GATA1, H3K27Ac, CTCF ChIP-Seq profiles and the DNaseI profile. The picture is representative of 2 technical duplicates.
c FLI-1 ChIP-Seq and differential contact profiles between Control and shFli-1 MEL cells (blue line) or between MEL cells and E14.5 mFL (orange line). The lines represent the log2 fold change of the aforementioned differences. The *Meis1* promoter is taken as a viewpoint.
d FLI-1 ChIP-Seq (black) and T2C plotted as 3C-Seq profile profile view of MEL cells expressing the control shRNA (dark colors) or shRNA against Fli-1 mRNA (medium colors) and E14.5 fetal liver cells (light colors) in the Fut8 locus. The Meis1 +94 enhancer (red profiles), Meis1 +55 (blue profiles) and Meis1 +48 (green profiles) are used as a viewpoint.
e FLI-1 ChIP-Seq (black) and 3C-Seq profile view of MEL cells expressing the control shRNA (dark blue) or shRNA against Fli-1 mRNA (light blue) and E14.5 fetal liver cells (red) in the Fut8 locus. The Fut8 promoter is used as a viewpoint.
f FLI-1 ChIP-Seq (black) and 3C-Seq profile view of MEL cells expressing the control shRNA (dark blue) or shRNA against Fli-1 mRNA (light blue) and E14.5 fetal liver cells (red) in the Fut8 locus. The Fut8 -140 region is used as a viewpoint.

Figure S4 (Related to Figure 4) : FLi-1 and the LDB1 complex directly activate the expression of megakaryocytic genes
a ChIP experiments using an anti-GATA-1 or an anti-LDB1 antibody or their respective control IgG performed in non-induced and induced MEL cells expressing a control shRNA (shSCR) or shRNA directed against Fli-1 mRNA (shFli-1) followed by qPCR to amplify the control region in the β-amylase locus (Amy, black bar) or the FLI-1 binding regions identified by ChIP-Seq (see Figure 1d) in the Gp1ba (blue bar) and the Cd41 promoter (red bar). The bars represent the geometric mean of the ratio between the FLI-1 binding regions and the control region of 3 independent experiments. The error bars represent the standard error. *: $p<0.05$ for the comparison between shSCR and shFli-1 MEL cells (paired t-test).

b, c (b) ChIP experiments performed with either the anti-FLI-1 antibody (blue bar) or the control IgG (black bar) in L8057 cells followed by qPCR to amplify the control region in the β -amylase locus (Amy) or the FLI-1 binding regions identified by ChIP-Seq (see Figure 1d) in the Gp1ba, Cd41 loci. The bars represent the geometric mean of the ratio between the FLI-1 binding regions and the control region of 3 independent experiments. The error bars represent the standard error.*: $p<0.05$ for the comparison between FLI-1 and control IgG (paired t-test). (c): ChIP experiments with antibodies against GATA-1 (red bars) or LDB1 (orange bars) or the control IgG (black bars) in L8057 cells followed by qPCR to amplify the control amylase region (Negative region), the Gp1ba promoter and the Cd41 promoter. The bars represent the geometric mean of the ratio between the FLI-1 binding regions and the control region (of 3 independent experiments. The error bars represent the standard error. * : p-value <0.05 for the comparison between FLI-1 binding regions and the negative region (paired t-test).
d Top panel: Genome view of the RNA-Seq reads of WT (bottom) or the FLI-1 KO MkP (top) displaying the absence of reads in the coding sequence of the Fli-1 exon 9 in the FLI-1 KO MkP. Bottom panel: Fli-1 RPKM value in WT (black bar) and FLI-1 KO (purple bar) MkP.
e Scheme of the protocol followed to analyze gene expression in megakaryocytes after Fli-1 and/or Lmo2 repression. cKit+ cells were isolated from E14.5 mouse fetal liver and infected with lentiviruses expressing either a control shRNA (shSCR) or shRNA targeting Fli-1 or Lmo2 or both mRNA. Cells were then cultured for 5 days in presence of mSCF and mTpo followed by 4 extra days in presence of only mTpo. RNA were isolated and RT-qPCR were performed to assess the mRNA levels of megakaryocytic genes (Figure 4f).
f Quantification by RT-qPCR analyses of the Fli-1 (left panel) and Lmo2 (right panel) mRNA levels from control mature megakaryocytes (black bars) or mature megakaryocytes knocked-down for Fli-1 (shFli-1, blue bars), or for Lmo2 (shLmo2, red bars) or both (purple bars). The
bars represent the geometric mean of 3 independent experiments. The error bars represent the standard errors. **: $p<0.01$ for the comparison with the shSCR condition (paired t-test).
g ChIP-Seq profiles for FLI-1, GATA1 and TAL1 and the Input control at the Gp1ba, Cd41, Selp, Rab27b and vWF loci in megakaryocytes.
h Fetal liver cells from E14.5 mouse embryos have been infected by lentiviruses expressing either control shRNA (shSCR, dark coloured bars) or shRNA against *Fli-1* mRNA (light coloured bars) and cultured for 3 days in presence of SCF and Tpo cytokines to prime megakaryopoiesis. Cells were then crosslinked and ChIP experiments were performed using either the anti-FLI-1 (blue bars), the anti-GATA1 (red bars) and the anti-LDB1 (orange bars) antibodies followed by qPCR experiments to amplify the negative region (in the β-amylase locus) and the promoters of *Gp1ba* and *Cd41* gene. The bars represent the fold enrichment relative to the control IgG that have been used in parallel.

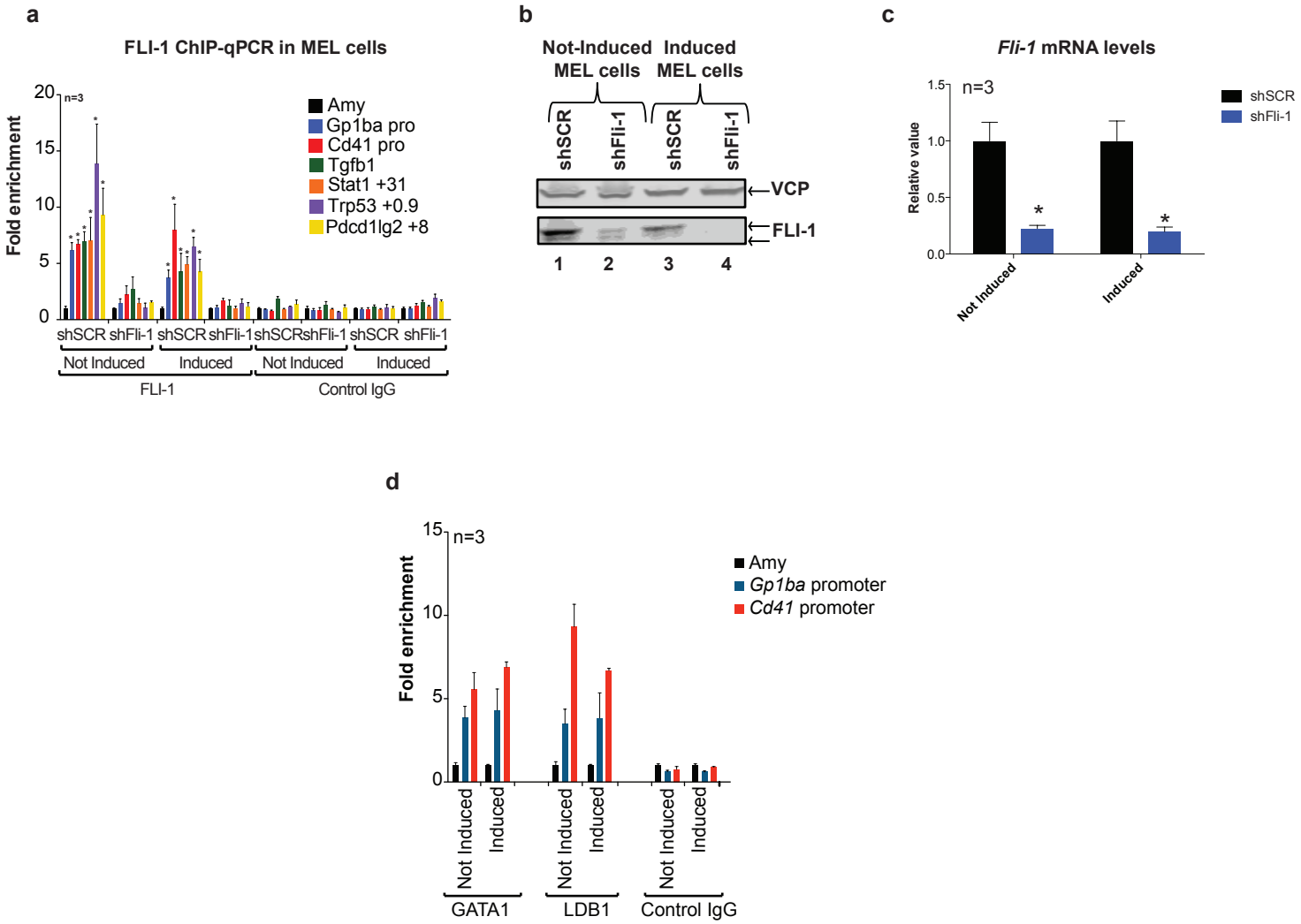
a
FLI-1 ChIP-qPCR in MEL cells
Fold enrichment
n=3
Amy
Gp1ba pro
Cd41 pro
Tgfb1
Stat1 +31
Trp53 +0.9
Pdcd1lg2 +8
shSCR shFli-1 shSCR shFli-1 shSCR shFli-1 shSCR shFli-1
Not Induced
Induced
Not Induced
Induced
FLI-1
Control IgG
b
Not-Induced MEL cells
Induced MEL cells
shSCR
shFli-1
shSCR
shFli-1
VCP
FLI-1
1 2 3 4
c
Fli-1 mRNA levels
n=3
Relative value
shSCR
shFli-1
Not Induced
Induced
d
n=3
Fold enrichment
Amy
Gp1ba promoter
Cd41 promoter
Not Induced
Induced
Not Induced
Induced
Not Induced
Induced
GATA1
LDB1
Control IgG

Figure S1

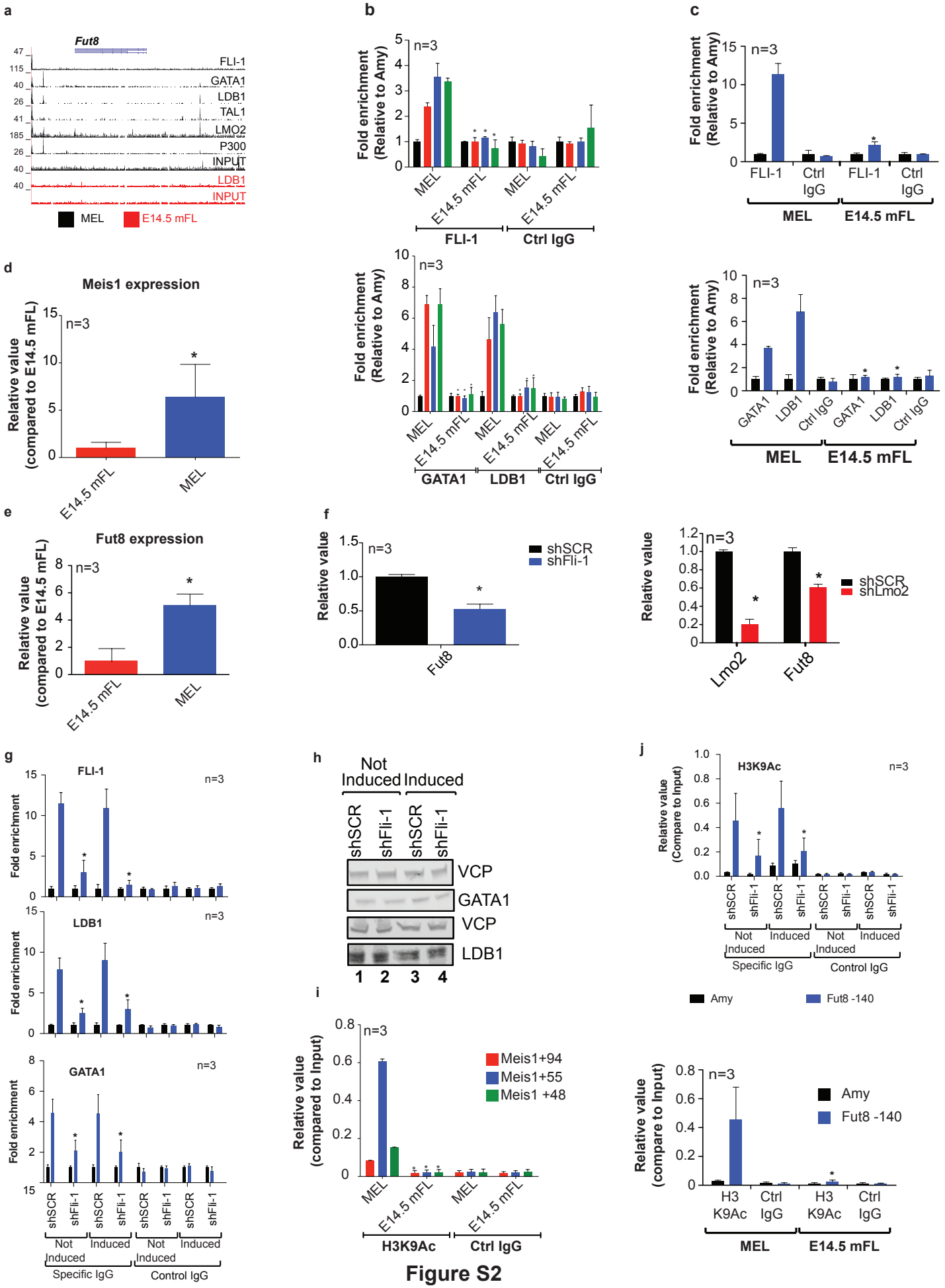
a
Fut8
FLI-1
GATA1
LDB1
TAL1
LMO2
P300
INPUT
LDB1
INPUT
MEL
E14.5 mFL
b
Fold enrichment (Relative to Amy)
n=3
MEL
E14.5 mFL
MEL
E14.5 mFL
FLI-1
Ctrl IgG
GATA1
LDB1
Ctrl IgG
c
Fold enrichment (Relative to Amy)
n=3
FLI-1
Ctrl IgG
FLI-1
Ctrl IgG
MEL
E14.5 mFL
GATA1
LDB1
Ctrl IgG
GATA1
LDB1
Ctrl IgG
MEL
E14.5 mFL
d
Meis1 expression
Relative value (compared to E14.5 mFL)
n=3
E14.5 mFL
MEL
e
Fut8 expression
Relative value (compared to E14.5 mFL)
n=3
E14.5 mFL
MEL
f
Relative value
n=3
shSCR
shFli-1
Fut8
Relative value
n=3
shSCR
shLmo2
Lmo2
Fut8
g
FLI-1
LDB1
GATA1
Fold enrichment
n=3
shSCR
shFli-1
Not Induced
Induced
Specific IgG
Control IgG
Amy
Fut8 -140
h
Not Induced
Induced
shSCR
shFli-1
VCP
GATA1
VCP
LDB1
1 2 3 4
i
Relative value (compared to Input)
n=3
Meis1+94
Meis1+55
Meis1 +48
MEL
E14.5 mFL
H3K9Ac
Ctrl IgG
j
H3K9Ac
Relative value (Compare to Input)
n=3
shSCR
shFli-1
Not Induced
Induced
Specific IgG
Control IgG
Amy
Fut8 -140
Relative value (compare to Input)
n=3
Amy
Fut8 -140
H3 K9Ac
Ctrl IgG
MEL
E14.5 mFL

Figure S2

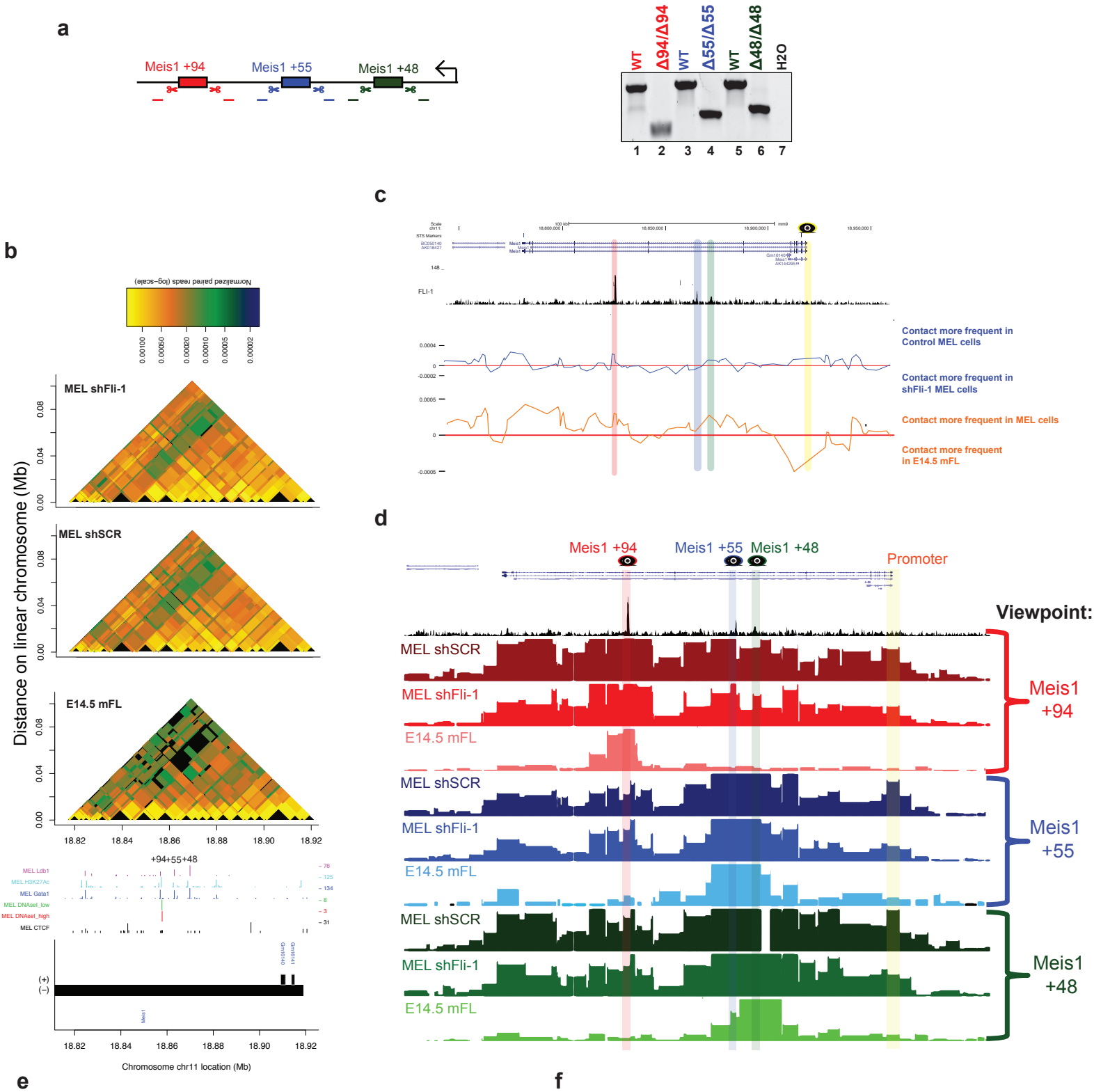
a
Meis1 +94
Meis1 +55
Meis1 +48
WT
Δ94/Δ94
WT
Δ55/Δ55
WT
Δ48/Δ48
H2O
1 2 3 4 5 6 7
b
Normalized paired reads (log-scale)
0.00100
0.00050
0.00020
0.00010
0.00005
0.00002
MEL shFli-1
MEL shSCR
E14.5 mFL
Distance on linear chromosome (Mb)
18.82 18.84 18.86 18.88 18.90 18.92
+94+55+48
MEL Ldb1
MEL H3K27Ac
MEL Gata1
MEL DNaseI_low
MEL DNaseI_high
MEL CTCF
Chromosome chr11 location (Mb)
c
FLI-1
Contact more frequent in Control MEL cells
Contact more frequent in shFli-1 MEL cells
Contact more frequent in MEL cells
Contact more frequent in E14.5 mFL
d
Meis1 +94
Meis1 +55
Meis1 +48
Promoter
Viewpoint:
MEL shSCR
MEL shFli-1
E14.5 mFL
Meis1 +94
Meis1 +55
Meis1 +48
e
Fut8
FLI-1 ChIP-Seq (MEL)
shSCR
shFli-1
E14.5 mFL
f
Fut8
FLI-1 ChIP-Seq (MEL)
MEL shSCR
MEL shFli-1
E14.5 mFL

Figure S3

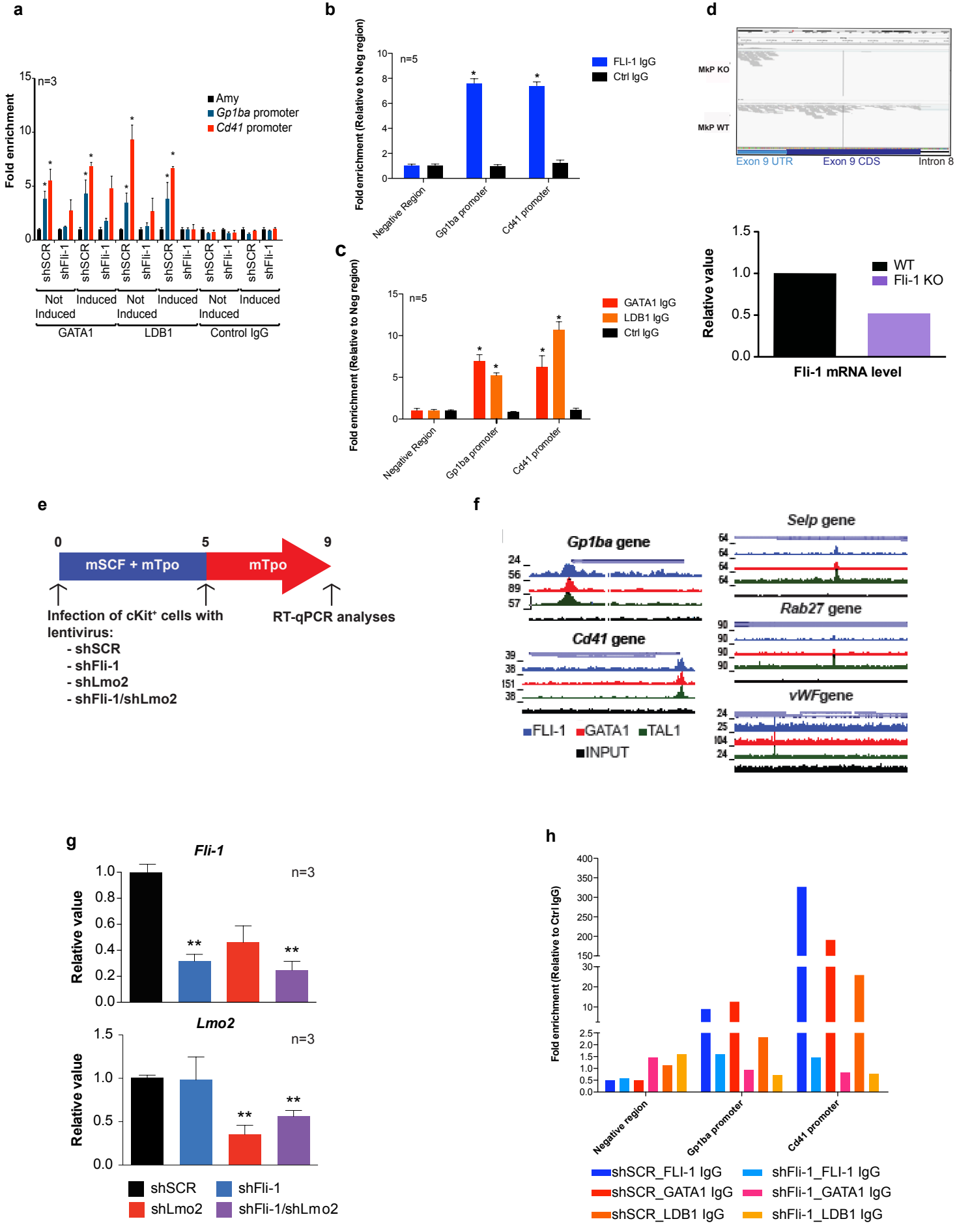
a
Fold enrichment
n=3
Amy
Gp1ba promoter
Cd41 promoter
shSCR
shFli-1
Not Induced
Induced
GATA1
LDB1
Control IgG
b
Fold enrichment (Relative to Neg region)
n=5
FLI-1 IgG
Ctrl IgG
Negative Region
Gp1ba promoter
Cd41 promoter
c
Fold enrichment (Relative to Neg region)
n=5
GATA1 IgG
LDB1 IgG
Ctrl IgG
d
MkP KO
MkP WT
Exon 9 UTR
Exon 9 CDS
Intron 8
Relative value
WT
Fli-1 KO
Fli-1 mRNA level
e
0
5
9
mSCF + mTpo
mTpo
Infection of cKit+ cells with lentivirus:
- shSCR
- shFli-1
- shLmo2
- shFli-1/shLmo2
RT-qPCR analyses
f
Gp1ba gene
Cd41 gene
Selp gene
Rab27 gene
vWFgene
FLI-1
GATA1
TAL1
INPUT
g
Fli-1
Lmo2
Relative value
n=3
shSCR
shFli-1
shLmo2
shFli-1/shLmo2
h
Fold enrichment (Relative to Ctrl IgG)
Negative region
Gp1ba promoter
Cd41 promoter
shSCR_FLI-1 IgG
shFli-1_FLI-1 IgG
shSCR_GATA1 IgG
shFli-1_GATA1 IgG
shSCR_LDB1 IgG
shFli-1_LDB1 IgG

Figure S4

SUPPLEMENTAL TABLE

Table S1 : List of antibodies used (Related to Figure 1, 2 3 and 4)

Antibody against	Techniques	Conjugated with	Brand	Reference
CD117	FACS	PE-Cy7	BioLegend	105813
		APC	BioLegend	105812
CD41	FACS	FITC	BioLegend	133903
CD61	FACS	PE	BioLegend	104307
TER119	FACS	Biotin	BioLegend	116203
SCA1	FACS	Biotin	BioLegend	108103
CD3	FACS	Biotin	BioLegend	100243
CD127	FACS	Biotin	BioLegend	135005
CD19	FACS	Biotin	BioLegend	101504
Streptavidin	FACS	APC	BioLegend	405207
CD150	FACS	PerCp-Cy5.5	BioLegend	115921
FLI-1	Western blot/ChIP	NA	Abcam	ab-15289
GATA1	Western blot/ChIP	NA	Santa Cruz Biotechnologies	sc-1234
LDB1	Western blot/ChIP	NA	Santa Cruz Biotechnologies	sc-11198
VCP	Western blot	NA	Abcam	ab-11433
Goat anti-mouse	Western blot	IRDye800CW	LiCOR	926-32210
Donkey anti-goat	Western blot	IRDye800CW	LiCOR	926-32214
Goat anti-rabbit	Western blot	IRDye800CW	LiCOR	926-32211
FLI-1	ChIP-Seq	NA	Santa Cruz Biotechnologies	sc-356
Rabbit IgG	ChIP-qPCR	NA	Santa Cruz Biotechnologies	sc-2027
Goat IgG	ChIP-qPCR	NA	Santa Cruz Biotechnologies	sc-2028

Table S2 : List of primers (Related to Figure 1, 2, 3 and 4)

Primers for RT-qPCR		
Genes	**Forward**	**Reverse**
Actb	AGCACAGCTTCTTTGCAG	GATGGAGGGGAATACAGC
Fli-1	GTCAATGTCAAGCGGGAGTA	ATGACTCTCCGTTCGTTGGT
Lmo2	GAAAGGAAGAGCCTGGAC	ATGGCTTTCAGGAAGTAGC
Gp1ba	TAGAGAGAAGGACCGAGTCA	GCTGGTCACTTTGGAGATAC
Cd41	CTGCTGACCCTGCTAGTTT	CCCTCTGCTGTCACTCTTC
Thbs1	CTCTGCTTTCACAATGGAGT	TTTTGCAGATGGTAACCGA
Selp	TGGAATGATGAACCCTGTTT	CAATGGTCTCGATGCACT
Rab27b	ATCCCAAATTCATCACCACA	ACCTTAAACGCTTTTCCTGA
vWF	TGCAGTTATCTCCTGGCT	AAACTCCCCAAGATACACAG
Meis1	ACGCTTTTTGTGACGCTTTT	TCCACTCGTTCAGGAGGAAC
Trp53	TGTCATCTTTTGTCCCTTCT	CTTATTGAGGGGAGGAGAGT
Pdcd1lg2	GGCCATAGTGATAATCCAGA	GAAGTCTCTTGAGGGTTTCC
Stat1	ACAGAAGGAGCTGGACAGTA	AAAAACATCTTGTGGAGCAG
Tgfb1	CGAAGCGGACTACTATGCTA	CGAATGTCTGACGTATTGAA
Primers for ChIP-qPCR		
Region	**Forward**	**Reverse**
β-Amylase	CTCCTTGTACGGGTTGGT	AATGATGTGCACAGCTGAA
Gp1ba pro	TCACAGGAGCTGATTATCAG	AGACAGACAGTCCTTTGGAG
Cd41 pro	CTCTTGAATGCTGTGATGTG	AGGAAGTGGGTAAATGTCCT
Tgfb1	GGTGTCAGTAGCTTCTCCAG	GAAATGGGGTGACATAGAGA

Meis1 +94	CTGGTGGCAAGAGTTACTTC	CCACTTGACTTTCTCCACA
Meis1 +55	GTTGAGGTTTAGGCACTCTG	AGAGGTTCTCACAGGAACAA
Meis1 +48	CACTGAGATAGGAACCTGGA	GCATTTCTTGTCACTTCCTC
Stat1 +31	CACACCCACTAGGACAAGTT	GTGTTATCACTCAGGCAGGT
Trp53 +0.9	GATTCTAGGCTGGTTCTGTG	TAAAACCGGATACTCGGTAA
E2f2 +5.7	AGAGTGTTTGCACTGTTTCC	GTGAGAGGCAAATAATCAGG
Dusp1 +5.5	AAAGGGAAACTCCTCAGTGT	GTCCGTGGTCTCAACTTAAC
Pdcd1lg2 +8	GATCAGGCTTTATTGCTCAC	TCTAGGCTCTTCAGTCTCCA
Primers for screening Meis1 CRISPR clones		
Viewpoint	**Forward**	**Reverse**
Meis1 ∆94	ATGTCTCAAAACAAACAAAAGC	TGGAGTCACCTTGGGATT
Meis1 ∆55	TCTGACTCACAATTGAAAAAGG	GCACAGAGCGTGTAGACG
Meis1 ∆48	CCCATCATGTAGCATTGTG	AGAGCAATGGAGATATTTGC
gRNA for deleting Meis1 enhancer		
	Sense	Antisense
5' Meis1 ∆94	GGTCTACAATAGCTCCTTCC	CGGAAGGAGCTATTGTAGAC
3' Meis1 ∆94	TGAGGGGTTAATGTTAGAGG	CCTCTAACATTAACCCCTCA
5' Meis1 ∆55	GCTATCTCACCCGACCCCCC	GGGGGGTCGGGTGAGATAGA
3' Meis1 ∆55	GCTGAGGAGGGTCGAGCCCT	AGGGCTCGACCCTCCTCAGC
5' Meis1 ∆48	ACTCAGGGCTGGCCGTTGGC	GCCAACGGCCAGCCCTGAGT
3' Meis1 ∆48	ACCTGCTGCTTTAGGTATTC	GAATACCTAAAGCAGCAGGT

TRANSPARENT METHODS

Mice
Ethical approval was obtained from the Committee on the Ethics of Animal Experiments (DEC) of the Erasmus MC as well as from the was obtained from the Ministère Délégué de la Recherche et des Nouvelles Technologies, agreement no. 4936; Direction des Services Vétérinaires, agreement n°69266317 and 7462.
All animal experiments were carried out according to institutional and national and EU guidelines.

Megakaryocyte differentiation, staining and transduction
Fetal liver cells were isolated from E14.5 embryos and homogenized to obtain a single-cell suspension. cKit $(CD117)^+$ cells were isolated by incubating the cells with biotin-conjugated CD117 antibody for 30 minutes followed by 30 minutes incubation with magnetic streptavidin microbeads (Miltenyi biotech) in a buffer containing PBS, 2 mM EDTA and 0.5 % biotin-free bovine serum albumin (Thermo Fisher). Cells were passed in a LS column (Miltenyi biotech) attached to a magnet, washed 3 times with a buffer containing PBS and 2 mM EDTA and the $cKit^+$ cells were collected by adding the plunger to the column. The positive population was then transduced with 20 µL of lentivirus in presence of 8 µg/mL polybrene and cultured for 5 days in IMDM (Life technologies) supplemented with 10 % FCS, 50 ng/mL mTPO, 10 ng/mL mSCF. Cells were then washed 5 times with IMDM, transduced with lentiviruses as above and cultured for 4 additional days in IMDM supplemented with 10 % FCS, 50 ng/mL mTPO.

Constructs
gRNAs targeting the *Meis1* enhancers (sequences in Table S1) were cloned in the BbsI site of the pX459 plasmid (gift from Feng Zhang Addgene plasmid # 62988) (Ran et al., 2013).

Isolation of MkP from WT and FLI-1 KO mice
MkP were isolated from the bone marrow of WT and FLI-1 KO mice following the protocol described by Pronk *et al.* and using a FACS Aria III (Pronk et al., 2007; Starck et al., 2010). The antibodies used are listed in Table S2.

Western blot
Western blot experiments were performed as described previously (Giraud et al., 2014). The primary and secondary antibodies used are listed in Table S1.

Chromatin immunoprecipitation (ChIP)
ChIP experiments were performed as described previously(Giraud et al., 2014). The antibodies used are listed in Table S1.

cDNA synthesis
500 ng of RNA isolated using the TRI Reagent (Sigma-Aldrich) was retro-transcribed into cDNA by using the SuperScript II First Strand Synthesis System (Life technologies) and oligo-dT primers (Life technologies) according to manufacturer's instruction.

Real-time PCR
Real-time PCR was performed using the platinum Taq Polymerase (Life technologies), SYBR green (Biorad) and the primers listed in Table S2 on a Biorad CFX96 apparatus. The specificity and the linear efficiency of each primer have been tested using different amount of mouse genomic DNA or mouse cDNA. Melting curves were checked to confirm the amplification of only the expected amplicon. A negative control was performed in parallel with the real experiment. For gene expression, qPCR reactions were performed in technical duplicates from 5 ng of cDNA and relative DNA levels were calculated using the $\Delta\Delta$Ct method and were normalized to the expression of the *Actb* RNA level. For ChIP, qPCR reactions were performed in technical duplicates from 1/25 of ChIP DNA solution and 1/67 of Input DNA solution. Relative DNA levels were calculated using the $\Delta\Delta$Ct method and were normalized to the Input level.

T2C
T2C experiments were performed as described(Kolovos et al., 2014, 2018) using HindIII as a first enzyme and DpnII as second enzyme. The visualization of the interactome of specific DNA fragments (viewpoints) was performed as described before(Kolovos et al., 2014, 2018).

3C-Seq
3C-Seq experiments were performed as described by Stadhouders *et al.* by using HindIII as first enzyme and NlaIII (*Fut8* enhancer as a viewpoint) or DpnII (*Fut8* promoter as a viewpoint) as second enzyme (Stadhouders et al., 2013). The primers used are listed in Table S1. The samples were sequenced in Illumina Hiseq2500. Raw data were mapped to the reference genome (mm9) and analyzed using the r3Cseq (Thongjuea et al., 2013).

Data availability
The accession number for the FLI-1 ChIP-Seq, the RNA-Seq and the T2C experiments reported in this paper is SRA: SRP158024.

Cell culture and treatment
MEL and HEK cells were cultured in DMEM medium (Lonza) supplemented with 10 % fetal calf serum and penicillin/streptomycin. Cells were induced with 2 % DMSO for 2 days. Expression of control shRNA or shRNAs against Fli-1 mRNA was induced by treating the cells with 100 ng/mL doxycyclin 2 days prior to DMSO treatment. L8057 cells were cultured in vol/vol IMDM/RPMI1640 (Life technologies) supplemented with10 % fetal calf serum and penicillin/streptomycin.

Lentivirus production
20 µg of pLKO.1 (containing the shRNA), 15 µg PAX2 and 5 µg VSV-G plasmids were incubated for 20 minutes with 100 µg PEI and applied to HEK cells. Cells were cultured for 4 hours in DMEM supplemented with 1 % FCS and then for 3 days in DMEM supplemented with 10 % FCS and penicillin/streptomycin. Each day, the medium containing the lentiviral particles was collected and stored at 4 °C. The collected medium was then centrifuged 5 minutes at 1500 rpm, passed through a 0.45 µm filter and ultra-centrifuged 2:15 hours at 20000 rpm at 4 °C. Supernatant was discarded and the lentivirus pellet was resuspended in 100 µL cold PBS. 20 µL were used to transduce cells in presence of 8 µg/mL polybrene.

ChIP in transduced fetal liver cells
Fetal liver cells were isolated from E14.5 embryos and homogenized to obtain a single-cell suspension. Cells were then transduced with 20 µL of lentivirus in presence of 8 µg/mL polybrene and cultured for 3 days in IMDM (Life technologies) supplemented with 10 % FCS, 50 ng/mL mTPO, 10 ng/mL mSCF. Cells were then crosslinked using 1 % formaldehyde and quenched with 0.125 M Glycine. Cells were lysed in a freshly made TE/NP40 buffer (10 mM Tris pH 8, 1 mM EDTA, 0.5 % NP-40, 1 X PIC (Roche Diagnostics)) for 10 minutes in ice. After a centrifugation of 5 minutes at 4 ˚C and 2500 g, the nuclei pellet was resuspend in the NEB buffer (50 mM Tris pH 8, 1 % SDS, 10 mM EDTA, 1 X PIC) and incubated for 10 minutes in ice. The chromatin was then sheared in the Bioruptor (Diagenode) during 30 minutes with the cycle 30 sec ON 30 sec OFF at high intensity. The sonicated chromatin was then precleared using Protein A/G coated agarose beads in the RIPA-150 buffer (50 mM Tris pH8, 0.15 M NaCl, 1 mM EDTA, 0.1 % SDS, 1 % Triton-X100, 0.1 % Na DOC) supplemented with 1 X PIC and 1 % BSA for 3 h at 4 ˚C. Beads were then discarded, new Protein A/G agarose beads attached to 5 µg of specific IgG were added to the pre-cleared chromatin and the mixture was incubated overnight at 4 ˚C. Beads were then washed once with RIPA-150 buffer, twice with RIPA-500 buffer (50 mM Tris pH8, 0.5 M NaCl, 1 mM EDTA, 0.1 % SDS, 1 % Triton-X100, 0.1 % Na DOC), twice with RIPA-$LiCl_2$ buffer (50 mM Tris pH 8, 1 mM EDTA, 1 % NP-40, 0.7 % Na DOC, 0.5 M $LiCl_2$) and twice with TE buffer (10 mM Tris pH 8, 1 mM EDTA). Chromatin was then eluted in Elution Buffer (1% SDS, 0.1 M $NaHCO_3$) and decrosslinked overnight at 65 ˚C. Proteins were then degraded by 20 µg Proteinase K for 1 h at 56 ˚C and chromatin was purified using Phenol:Chloroform, precipitated with 1 volume of isopropanol and washed once with 70 % EtOH.

ChIP-Seq
The samples were sequenced at Illumina Hiseq2500. Raw read files were aligned to the mouse genome (NCBI build 37; mm9) using Bowtie (Langmead et al., 2009) and discarding reads mapping to multiple genomic locations. Data processing and analysis were mainly performed as previously described (Soler et al., 2011 ; Stadhouders et al., 2015 ; Kolovos et al., 2016). The ShortRead package (Morgan et al., 2009) was used to convert these into genome-wide coverage files. Using negative binomial distributions, we assigned P-values and false discovery rates (FDR) to each binding region (Rozowsky et al., 2009), and the final peak lists were compiled according with the following criteria: ≥20 read counts at each peak summit and FDR ≤0.001 (using non-specific, IgG, ChIP-seq data as background). Overlaps between binding peaks in the different datasets were identified using

the “findOverlaps” function from the GenomicRanges suite, while the iRanges package (Lawrence et al., 2013) was used in custom R scripts for annotating the genomic location of peaks and defining the closest gene to each. For motif analysis, +/- 100 bp from the centre of the peaks were selected using the rGADEM Bioconductor package (Droit et al., 2010), which then compares discovered sequences to the Jaspar database (Khan et al., 2018) based on similarity score with TOMTOM (Gupta et al., 2007).
FLI-1, GATA1 and TAL1 ChIP-seq in megakaryocytes were acquired from the ENCODE database (Pimkin et al., 2014; Yue et al., 2014) and analyzed as previously described.The coordinates of the FLI-1 total binding regions and common binding regions in MEL cells and in Megakaryocytes are listed in **Table S3**.

RNA-Seq
RNA were isolated with either the miRNeasy Mini Kit (QIAGEN) (for MEL cells) or miRNeasy MicroKit (QIAGEN) (for MkP) according to manufacturer’s instructions. The samples were sequenced at Illumina Hiseq2500. Reads were aligned to the mouse genome (NCBI build 37; mm9) using Tophat (Trapnell et al., 2009) and default parameters (“no-coverage-search”, “segment-length 18” as input options) while reads that did not map uniquely were discarded. Uniquely mapped reads were counted per RefSeq gene exon using HTseq (Anders et al., 2015) and statistical analysis of differentially-expressed genes was performed via DESeq (Anders and Huber, 2010). In all cases up- and downregulated genes were selected to have at least ±0.6 log2 fold-change in RNA levels. GO analysis was performed by PANTHER (Mi et al., 2019). The list of mis-regulated genes in MEL cells and in MkP after FLI-1 repression are listed in **Table S4**.

SUPPLEMENTAL REFERENCES

Anders S, Huber W. 2010. Differential expression analysis for sequence count data. Genome Biol 11:R106.

Anders S, Pyl PT, Huber W. HTSeq--a Python framework to work with high-throughput sequencing data. Bioinformatics. 2015 Jan 15;31(2):166-9

Droit A, Gottardo R, Robertson G, Li L (2018). rGADEM: de novo motif discovery. R package version 2.30.0.

Gupta S, Stamatoyannopoulos JA, Bailey TL, Noble W. 2007. Quantifying similarity between motifs. Genome Biology 8:R24.

Khan A, Fornes O, Stigliani A, Gheorghe M, Castro-Mondragon JA, van der Lee R, Bessy A, Chèneby J, Kulkarni SR, Tan G, Baranasic D, Arenillas DJ, Sandelin A, Vandepoele K, Lenhard B, Ballester B, Wasserman WW, Parcy F, Mathelier A. JASPAR 2018: update of the open-access database of transcription factor binding profiles and its web framework. Nucleic Acids Res. 2018 Jan 4;46(D1):D260-D266.

Lawrence M, Huber W, Pagès H, Aboyoun P, Carlson M, Gentleman R, Morgan MT, Carey VJ. 2013. Software for Computing and Annotating Genomic Ranges. PLoS Computational Biology 9:e1003118.

Mi H, Muruganujan A, Ebert D, Huang X, Thomas PD. 2019. PANTHER version 14: more genomes, a new PANTHER GO-slim and improvements in enrichment analysis tools. Nucleic Acids Research 47:D419–D426.

Morgan M, Anders S, Lawrence M, Aboyoun P, Pages H, Gentleman R. 2009. ShortRead: a bioconductor package for input, quality assessment and exploration of highthroughput sequence data. Bioinformatics 25:2607–2608.

Rozowsky J, Euskirchen G, Auerbach RK, Zhang ZD, Gibson T, Bjornson R, Carriero N, Snyder M, Gerstein MB. 2009. PeakSeq enables systematic scoring of ChIP-seq experiments relative to controls. Nature Biotechnology 27:66–75.

Soler E, Andrieu-Soler C, Boer E, Bryne JC, Thongjuea S, Rijkers E, Demmers J, van IW, Grosveld F. 2011. A systems approach to analyze transcription factors in mammalian cells. *Methods* **53**: 151-162.

Stadhouders R, Cico A, Stephen T, Thongjuea S, Kolovos P, Baymaz HI, Yu X, Demmers J, Bezstarosti K, Maas A et al. 2015. Control of developmentally primed erythroid genes by combinatorial co-repressor actions. *Nat Commun* **6**: 8893.

Thongjuea, S., Stadhouders, R., Grosveld, F.G., Soler, E., and Lenhard, B. (2013). r3Cseq: an R/Bioconductor package for the discovery of long-range genomic interactions from chromosome conformation capture and next-generation sequencing data. Nucleic Acids Res. *41*, e132**.**

Trapnell C, Pachter L, Salzberg SL. 2009. TopHat: discovering splice junctions with RNASeq. Bioinformatics 25:1105–1111.

Zhang Y, Liu T, Meyer CA, Eeckhoute J, Johnson DS, Bernstein BE, Nussbaum C, Myers RM, Brown M, Li W, Liu XS. 2008. Model-based Analysis of ChIP-Seq (MACS). Genome Biology 9:R137.